

Spinwave damping in the two-dimensional ferromagnetic XY model

G. M. Wysin,* M. E. Gouvêa, and A. S. T. Pires

Departamento de Física, ICEx, Universidade Federal de Minas Gerais Belo Horizonte,
CP 702, CEP 30123-970, MG, Brazil

(December 6, 1999)

The effect of damping of spinwaves in a two-dimensional classical ferromagnetic XY model is considered. The damping rate $\Gamma_{\mathbf{q}}$ is calculated using the leading diagrams due to the quartic-order deviations from the harmonic spin Hamiltonian. The resulting four-dimensional integrals are evaluated by extending the techniques developed by Gilat and others for spectral density types of integrals. $\Gamma_{\mathbf{q}}$ is included into the memory function formalism due to Reiter and Solander, and Menezes, to determine the dynamic structure function $S(\mathbf{q}, \omega)$. For the infinite sized system, the memory function approach is found to give non-divergent spinwave peaks, and a smooth nonzero background intensity (“plateau” or distributed intensity) for the whole range of frequencies below the spinwave peak. The background amplitude relative to the spinwave peak rises with temperature, and eventually becomes higher than the spinwave peak, where it appears as a central peak. For finite-sized systems, there are multiple sequences of weak peaks on both sides of the spinwave peaks whose number and positions depend on the system size and wavevector in integer units of $2\pi/L$. These dynamical finite size effects are explained in the memory function analysis as due to either spinwave difference processes below the spinwave peak or sum processes above the spinwave peak. These features are also found in classical Monte Carlo – Spin-Dynamics simulations.

PACS numbers: 75.10.Hk, 75.30.Ds, 75.40.Gb, 75.40.Mg

I. INTRODUCTION

The two-dimensional (2D) ferromagnetic XY model has had a long history of studies concerning the dynamics of spinwaves at low temperatures. It was first analyzed by Villain¹ and by Moussa and Villain², for low temperatures, in the harmonic approximation. They found that the dynamic structure function $S(\mathbf{q}, \omega)$ has a spinwave peak of the form

$$S(\mathbf{q}, \omega) \sim |\omega - \omega_{\mathbf{q}}|^{-1+\eta/2}, \quad (1)$$

where η is the critical exponent describing the decay of the static spin-spin correlation function, and $\omega_{\mathbf{q}}$ is the spinwave frequency at wavevector \mathbf{q} . Nelson and Fisher³ treated the model in a fixed-length hydrodynamic description, obtaining the following expression around the spinwave peak,

$$S(\mathbf{q}, \omega) \sim \frac{1}{q^{3-\eta}} \frac{1}{|1 - \omega^2/\omega_{\mathbf{q}}^2|^{1-\eta}}, \quad (2)$$

where for small q , $\omega_{\mathbf{q}} = cq$, with c being the spinwave velocity. These theoretical approaches led to spinwave peaks diverging unphysically at the spinwave frequency. Here we describe an alternative theoretical description in which the divergence does not occur.

At higher temperatures, the spinwave or harmonic approximation begins to fail, and XY magnets are known to undergo a topological phase transition^{4,5} associated with the unbinding of vortices. We generally consider temperatures below this unbinding temperature T_{BKT} , where a spinwave approximation will be valid. At very low temperatures any nonlinear effects should be very weak, do not lead to vortex production, and can be included as the damping or scattering of the spinwave modes, that results in a spinwave lifetime. Thus our approach will be to start from the harmonic approximation to the spin Hamiltonian, H_0 , and then include the damping that results from the terms fourth order in spin operators (H_1) in an expansion of the original full spin Hamiltonian, H . The resulting damping strength $\Gamma_{\mathbf{q}}$ will imply a finite lifetime $\tau = \Gamma_{\mathbf{q}}^{-1}$ for the spinwave modes. We are interested to investigate whether the presence of such lifetime effects can eliminate the divergence of the dynamic structure function $S(\mathbf{q}, \omega)$ at the spinwave frequency.

We calculate the spinwave damping by a Feynmann diagram technique for finite temperatures, applied to the fourth-order Hamiltonian H_1 , using the leading diagrams to second order in H_1 . The only diagrams we include are those that give a contribution to the *imaginary part* of the spinwave energy, i.e., to the damping or inverse lifetime. These are the terms that involve a *dynamical* effect on the spinwave energies. The associated integral expressions for these diagrams require the evaluation of four-dimensional integrals involving a delta-function. Methods for evaluating this type of integral in three dimensions have been developed by Gilat and co-workers; here we show how to extend their work and apply the same technique in four dimensions.

In principle, we could also use the Feynmann technique to determine the leading changes in the *real part* of the spinwave energy, $\Delta\omega_{\mathbf{q}}$, due to the perturbation H_1 . This real part would result as the usual effect due to finite temperature: a shift in the spinwave frequencies to lower values as the temperature increases. It is essentially a *static* effect, primarily due to the renormalization of the nearest neighbor exchange interaction strength J with temperature. Calculation of these spinwave frequency shifts by the Feynmann technique would require including diagrams first order in H_1 ; the so-called

single-loop diagrams. In this paper, however, we are primarily concerned with accounting for dynamical effects. We will include the renormalization of the spinwave energies using the memory function formalism, combined with some input information from classical Monte Carlo (MC) data. In the memory function approach, the position of the spinwave peak in $S(\mathbf{q}, \omega)$ does not occur exactly at the zero-temperature dispersion relation, $\omega_{\mathbf{q}}$, but rather, close to the value $\sqrt{\langle \omega^2 \rangle_{\mathbf{q}}} < \omega_{\mathbf{q}}$, where $\langle \omega^2 \rangle_{\mathbf{q}}$ is the temperature-dependent second moment. $\langle \omega^2 \rangle_{\mathbf{q}}$ can be estimated from static quantities, either using low-temperature analytic expressions or results from Monte Carlo, the latter being necessary for temperatures approaching T_{BKT} . The memory function approach already includes to leading order the exchange strength renormalization, as can be seen in the shift in the position of the spinwave peaks. Thus we use it rather than making any renormalization of the exchange J .

A few comments can be made about how the damping $\Gamma_{\mathbf{q}}$ is included into the memory function calculation. Note that the damping calculation sketched above is completely independent of the memory function calculation; the latter is a formalism for calculating dynamic correlations for a given Hamiltonian and operators. Due to the XY symmetry of the model, the natural coordinates of the spins are the in-plane angle ϕ and out-of-plane spin component S^z . Fourier transforming and using a standard canonical transformation, the Hamiltonian is written in terms of creation and annihilation operators $a_{\mathbf{q}}^\dagger$ and $a_{\mathbf{q}}$, with time dependencies varying as $e^{i\omega_{\mathbf{q}}t}$ and $e^{-i\omega_{\mathbf{q}}t}$, respectively. Once damping is included, the time dependencies become $e^{i(\omega_{\mathbf{q}}+i\Gamma_{\mathbf{q}})t}$ and $e^{-i(\omega_{\mathbf{q}}-i\Gamma_{\mathbf{q}})t}$, respectively. Henceforth the calculation proceeds as usual in the memory function approach, except for this small modification of the operator time dependencies via the shifted operator frequencies, $\omega_{\mathbf{q}} \rightarrow \omega_{\mathbf{q}} \pm i\Gamma_{\mathbf{q}}$.

In the memory function calculation, spinwave sum and difference processes enter. These are characterized by combinations of frequencies, $\Omega_{\pm} = \omega_{\frac{\mathbf{q}}{2}+\mathbf{k}} \pm \omega_{\frac{\mathbf{q}}{2}-\mathbf{k}}$, where \mathbf{q} is the wavevector at which the dynamic correlations are measured, and \mathbf{k} is summed over to include all possible such processes. Based on the above modifications of the operator frequencies, there also results the modification for these processes, $\Omega_{\pm} \rightarrow \Omega_{\pm} + i(\Gamma_{\frac{\mathbf{q}}{2}+\mathbf{k}} + \Gamma_{\frac{\mathbf{q}}{2}-\mathbf{k}})$. The damping rates for different wavevectors always add for both types of processes.

The paper is organized as follows: First, in Sec. II, we present the model and develop the expansion of the Hamiltonian to quartic order in creation/annihilation operators. In Sec. III, the expressions for the damping via the Feynmann technique are presented. Then we show how these are evaluated using the Gilat procedure. In Sec. IV, the key aspects of the memory function calculation of $S(\mathbf{q}, \omega)$ are reviewed, together with a focus on the modification due to the damping. Some details of the Monte Carlo and spin dynamics simulations are summarized in Sec. V. This is followed in Sec. VI by presentation

of the results both for very large and relatively smaller systems, in order to discuss the dynamical finite size effects. The memory function results also are compared with standard Monte Carlo – spin-dynamics calculations of the dynamic correlation functions in order to evaluate the validity and accuracy of the method. Our conclusions are presented in Sec. VII.

II. THE MODEL

The ferromagnetic spin Hamiltonian under consideration is

$$H = -\frac{J}{2} \sum_{\mathbf{n}} \sum_{\mathbf{a}} (S_{\mathbf{n}}^x S_{\mathbf{n}+\mathbf{a}}^x + S_{\mathbf{n}}^y S_{\mathbf{n}+\mathbf{a}}^y + \lambda S_{\mathbf{n}}^z S_{\mathbf{n}+\mathbf{a}}^z) , \quad (3)$$

where the first sum is over all sites \mathbf{n} of a 2D square lattice, the second is over all nearest neighbor displacements \mathbf{a} , J is the nearest neighbor coupling strength, and each $\mathbf{S}_{\mathbf{n}}$ is a three-component classical spin-vector. Because each bond is counted twice, a factor of $\frac{1}{2}$ is included on J . We primarily concentrate on the XY model, with anisotropy parameter $\lambda = 0$, however, for completeness, formulas covering the easy-plane anisotropy range, $0 \leq \lambda < 1$, are presented.

A. Expansion of Hamiltonian

In order to develop the damping as a perturbation of the harmonic approximation, we need to expand the full spin Hamiltonian, including the harmonic (quadratic) and quartic deviations from the ground state. The ground state corresponds to spins aligned in any direction within the XY plane. Writing the spins in Hamiltonian (3) using coordinates $\phi_{\mathbf{n}}$ and $z_{\mathbf{n}}$,

$$\mathbf{S}_{\mathbf{n}} = S(\sqrt{1-z_{\mathbf{n}}^2} \cos \phi_{\mathbf{n}}, \sqrt{1-z_{\mathbf{n}}^2} \sin \phi_{\mathbf{n}}, z_{\mathbf{n}}) , \quad (4)$$

the Hamiltonian becomes

$$H = -\frac{JS^2}{2} \sum_{\mathbf{n}, \mathbf{m}} \left[\sqrt{(1-z_{\mathbf{n}}^2)(1-z_{\mathbf{m}}^2)} \cos(\phi_{\mathbf{n}} - \phi_{\mathbf{m}}) + \lambda z_{\mathbf{n}} z_{\mathbf{m}} \right] , \quad (5)$$

where we use a simplified notation for the nearest neighbors, $\mathbf{m} = \mathbf{n} + \mathbf{a}$. At low temperature, it is reasonable to expand for small $z_{\mathbf{n}}$ and $(\phi_{\mathbf{n}} - \phi_{\mathbf{m}})$, keeping up to quartic order in these, obtaining,

$$H = H_0 + H_1 \quad (6)$$

where the harmonic and quartic Hamiltonians are

$$H_0 = -\frac{JS^2}{2} \sum_{\mathbf{n}, \mathbf{m}} \left[1 + \lambda z_{\mathbf{n}} z_{\mathbf{m}} - \frac{1}{2}(z_{\mathbf{n}}^2 + z_{\mathbf{m}}^2) - \frac{1}{2}(\phi_{\mathbf{n}} - \phi_{\mathbf{m}})^2 \right] , \quad (7)$$

$$H_1 = \frac{JS^2}{2} \sum_{\mathbf{n}, \mathbf{m}} \left[\frac{1}{8} (z_{\mathbf{n}}^4 + z_{\mathbf{m}}^4 - 2z_{\mathbf{n}}^2 z_{\mathbf{m}}^2) - \frac{1}{4} (z_{\mathbf{n}}^2 + z_{\mathbf{m}}^2) (\phi_{\mathbf{n}} - \phi_{\mathbf{m}})^2 - \frac{1}{4!} (\phi_{\mathbf{n}} - \phi_{\mathbf{m}})^4 \right]. \quad (8)$$

It is convenient to carry out the calculations in wavevector space by defining Fourier transforms

$$\phi_{\mathbf{n}} = \frac{1}{\sqrt{N}} \sum_{\mathbf{q}} e^{i\mathbf{q} \cdot \mathbf{n}} \phi_{\mathbf{q}}, \quad (9)$$

together with a similar definition for $z_{\mathbf{q}}$. Here \mathbf{q} denotes a two-dimensional wavevector, the sums are over the first Brillouin zone (BZ), and N is the total number of lattice sites. Then we rewrite H_0 and H_1 as

$$H_0 = 2JS^2 \sum_{\mathbf{q}} [(1 - \gamma_{\mathbf{q}}) \phi_{\mathbf{q}} \phi_{-\mathbf{q}} + (1 - \lambda \gamma_{\mathbf{q}}) z_{\mathbf{q}} z_{-\mathbf{q}}], \quad (10)$$

and

$$H_1 = \frac{JS^2}{N} \sum_{\mathbf{q}_1, \mathbf{q}_2, \mathbf{q}_3, \mathbf{q}_4} \left\{ \frac{1}{2} (1 - \gamma_{\mathbf{q}_1 + \mathbf{q}_2}) z_{\mathbf{q}_1} z_{\mathbf{q}_2} z_{\mathbf{q}_3} z_{\mathbf{q}_4} - (1 + \gamma_{\mathbf{q}_3 + \mathbf{q}_4} - \gamma_{\mathbf{q}_3} - \gamma_{\mathbf{q}_4}) z_{\mathbf{q}_1} z_{\mathbf{q}_2} \phi_{\mathbf{q}_3} \phi_{\mathbf{q}_4} - \frac{1}{6} (1 + \gamma_{\mathbf{q}_1 + \mathbf{q}_2} + \gamma_{\mathbf{q}_1 + \mathbf{q}_3} + \gamma_{\mathbf{q}_1 + \mathbf{q}_4} - \gamma_{\mathbf{q}_1} - \gamma_{\mathbf{q}_2} - \gamma_{\mathbf{q}_3} - \gamma_{\mathbf{q}_4}) \phi_{\mathbf{q}_1} \phi_{\mathbf{q}_2} \phi_{\mathbf{q}_3} \phi_{\mathbf{q}_4} \right\}. \quad (11)$$

For the square lattice, with coordination number $z = 4$, the $\gamma_{\mathbf{q}}$ function

$$\gamma_{\mathbf{q}} = \frac{1}{z} \sum_{\mathbf{a}} e^{i\mathbf{q} \cdot \mathbf{a}} = \frac{1}{2} (\cos q_x + \cos q_y) \quad (12)$$

is an even function of \mathbf{q} , i.e., $\gamma_{\mathbf{q}} = \gamma_{-\mathbf{q}}$. The sums in (11) are constrained to $\mathbf{q}_1 + \mathbf{q}_2 + \mathbf{q}_3 + \mathbf{q}_4 = 0$.

Using the following canonical transformation to creation/annihilation operators,

$$\phi_{\mathbf{q}} = \alpha_{\mathbf{q}} (a_{\mathbf{q}}^{\dagger} + a_{-\mathbf{q}}), \quad z_{\mathbf{q}} = i\beta_{\mathbf{q}} (a_{\mathbf{q}}^{\dagger} - a_{-\mathbf{q}}), \quad (13)$$

$$\alpha_{\mathbf{q}} = \left[\frac{1 - \lambda \gamma_{\mathbf{q}}}{4S^2(1 - \gamma_{\mathbf{q}})} \right]^{1/4}, \quad \beta_{\mathbf{q}} = \left[\frac{1 - \gamma_{\mathbf{q}}}{4S^2(1 - \lambda \gamma_{\mathbf{q}})} \right]^{1/4}, \quad (14)$$

the quadratic Hamiltonian is diagonalized,

$$H_0 = \sum_{\mathbf{q}} \omega_{\mathbf{q}} \left[a_{\mathbf{q}}^{\dagger} a_{\mathbf{q}} + \frac{1}{2} \right], \quad (15)$$

$$\omega_{\mathbf{q}} = 4JS \sqrt{(1 - \gamma_{\mathbf{q}})(1 - \lambda \gamma_{\mathbf{q}})}. \quad (16)$$

The diagonal parts of H_1 can then be written as

$$H_1 = \sum_{\mathbf{q}_1 + \mathbf{q}_2 + \mathbf{q}_3 + \mathbf{q}_4 = 0} A(\mathbf{q}_1, \mathbf{q}_2, \mathbf{q}_3, \mathbf{q}_4) a_{\mathbf{q}_1}^{\dagger} a_{\mathbf{q}_2}^{\dagger} a_{-\mathbf{q}_3} a_{-\mathbf{q}_4}, \quad (17)$$

where

$$A(\mathbf{q}_1, \mathbf{q}_2, \mathbf{q}_3, \mathbf{q}_4) = \frac{JS^2}{N} \left\{ \begin{aligned} & \beta_{\mathbf{q}_1} \beta_{\mathbf{q}_2} \beta_{\mathbf{q}_3} \beta_{\mathbf{q}_4} (3 - \gamma_{\mathbf{q}_1 + \mathbf{q}_2} - \gamma_{\mathbf{q}_1 + \mathbf{q}_3} - \gamma_{\mathbf{q}_1 + \mathbf{q}_4}) \\ & - 3\beta_{\mathbf{q}_1} \alpha_{\mathbf{q}_2} \alpha_{\mathbf{q}_3} \beta_{\mathbf{q}_4} (1 + \gamma_{\mathbf{q}_2 + \mathbf{q}_3} - \gamma_{\mathbf{q}_2} - \gamma_{\mathbf{q}_3}) \\ & - \beta_{\mathbf{q}_2} \alpha_{\mathbf{q}_1} \alpha_{\mathbf{q}_4} \beta_{\mathbf{q}_3} (1 + \gamma_{\mathbf{q}_1 + \mathbf{q}_4} - \gamma_{\mathbf{q}_1} - \gamma_{\mathbf{q}_4}) \\ & + \beta_{\mathbf{q}_3} \alpha_{\mathbf{q}_1} \alpha_{\mathbf{q}_2} \beta_{\mathbf{q}_4} (1 + \gamma_{\mathbf{q}_1 + \mathbf{q}_2} - \gamma_{\mathbf{q}_1} - \gamma_{\mathbf{q}_2}) \\ & + \beta_{\mathbf{q}_1} \alpha_{\mathbf{q}_3} \alpha_{\mathbf{q}_4} \beta_{\mathbf{q}_2} (1 + \gamma_{\mathbf{q}_3 + \mathbf{q}_4} - \gamma_{\mathbf{q}_3} - \gamma_{\mathbf{q}_4}) \\ & - \alpha_{\mathbf{q}_1} \alpha_{\mathbf{q}_2} \alpha_{\mathbf{q}_3} \alpha_{\mathbf{q}_4} (1 + \gamma_{\mathbf{q}_1 + \mathbf{q}_2} + \gamma_{\mathbf{q}_1 + \mathbf{q}_3} + \gamma_{\mathbf{q}_1 + \mathbf{q}_4} \\ & - \gamma_{\mathbf{q}_1} - \gamma_{\mathbf{q}_2} - \gamma_{\mathbf{q}_3} - \gamma_{\mathbf{q}_4}) \end{aligned} \right\}. \quad (18)$$

We have dropped terms in H_1 whose expectation values in the ground state are zero. Note also that if a particular \mathbf{q}_i is zero, then $\alpha_{\mathbf{q}_i}$ diverges, however, when this occurs the corresponding factors multiplying $\alpha_{\mathbf{q}_i}$ go to zero faster, canceling the divergence.

III. SPINWAVE DAMPING DUE TO H_1

The time evolution of the creation/annihilation operators as given from the harmonic Hamiltonian is

$$a_{\mathbf{q}}^{\dagger}(t) = a_{\mathbf{q}}^{\dagger}(0) e^{i\omega_{\mathbf{q}} t}, \quad a_{\mathbf{q}}(t) = a_{\mathbf{q}}(0) e^{-i\omega_{\mathbf{q}} t}. \quad (19)$$

As discussed in the Introduction, the effect of the H_1 perturbation is to shift the spinwave frequencies, in the most general case, by some complex self-energy $\Sigma_{\mathbf{q}}$. For the moment, we ignore the real part of $\Sigma_{\mathbf{q}}$, whose effect will be included by the memory function approach, and concentrate instead on the contributions to the imaginary part of $\Sigma_{\mathbf{q}}$, which determine the spinwave damping. To find $\Sigma_{\mathbf{q}}$, the contributions of H_1 to the single particle Green's function will be evaluated, keeping only the diagrams that have a nonzero imaginary part. The lowest order diagrams that satisfy this requirement are found to be second order in H_1 ; there is no contribution from first order diagrams.

Following the standard procedure,⁶⁻⁸ the time-ordered zero-temperature Green's function, in second order, is

$$iG_2(\mathbf{k}_2, \mathbf{k}_1, t_2 - t_1) = \frac{(-i)^2}{2!} \int_{-\infty}^{\infty} dt'_1 \int_{-\infty}^{\infty} dt'_2 \times \langle \Phi_0 | T \{ H_1(t'_1) H_1(t'_2) a_{\mathbf{k}_2}(t_2) a_{\mathbf{k}_1}^{\dagger}(t_1) \} | \Phi_0 \rangle. \quad (20)$$

Here T is the time ordering operator, and Φ_0 is the ground state of H_0 . Physically, this Green function represents the amplitude for a quasiparticle (i.e., spinwave) created at time t_1 in state \mathbf{k}_1 to be destroyed at time t_2 in state \mathbf{k}_2 , after undergoing two scattering events due to H_1 . The free-particle Green function,

$$iG_0(\mathbf{k}_2, \mathbf{k}_1, t_2 - t_1) = \langle \Phi_0 | T \{ a_{\mathbf{k}_2}(t_2) a_{\mathbf{k}_1}^\dagger(t_1) \} | \Phi_0 \rangle, \quad (21)$$

involves no scattering. Due to momentum conservation, these Green functions are proportional to the Kronecker delta, $\delta_{\mathbf{k}_1, \mathbf{k}_2}$, so we can drop the double momentum indices. Also, because of time translational invariance, they depend only on the time difference $t = t_2 - t_1$. Introducing the time Fourier transforms,

$$G_n(\mathbf{k}, t) = \frac{1}{2\pi} \int_{-\infty}^{\infty} d\omega G_n(\mathbf{k}, \omega) e^{-i\omega t}, \quad (22)$$

the free propagator becomes the well-known expression,

$$G_0(\mathbf{k}, \omega) = \frac{1}{\omega - \omega_{\mathbf{k}} + i\delta}, \quad (23)$$

where $\delta = 0^+$.

We apply the rules for Feynmann diagrams to evaluate the full propagator, $G(\mathbf{k}, \omega)$, in terms of G_0 and G_2 . The free propagator $G_0(\mathbf{k}, \omega)$ is represented as a straight line with an associated momentum \mathbf{k} and frequency ω . The interaction term in (17) is represented as a wavy line as in Fig. 1, with an outgoing straight line (free propagator) for each creation operator and an incoming straight line for each destruction operator, both with assigned momentum and frequency. The two leading diagrams that contribute to $G_2(\mathbf{k}, \omega)$ are shown in Fig. 2. Following the standard Feynmann rules for these diagrams, with summations over the intermediate frequencies and wavevectors, and using momentum and frequency conservation at each junction, $G_2(\mathbf{k}, \omega)$ can be written as

$$G_2(\mathbf{k}, \omega) = G_0(\mathbf{k}, \omega) \Sigma(\mathbf{k}, \omega) G_0(\mathbf{k}, \omega), \quad (24)$$

where the self-energy function due to the scattering parts of the diagrams is

$$\begin{aligned} \Sigma(\mathbf{k}, \omega) = & -4 \sum_{\mathbf{p}, \mathbf{q}} \int \frac{d\omega'}{2\pi} \int \frac{d\omega''}{2\pi} \\ & G_0(\mathbf{q}, \omega'') G_0(\mathbf{p}, \omega' - \omega) G_0(\mathbf{k} + \mathbf{p} - \mathbf{q}, \omega' - \omega'') \\ & A(\mathbf{q}, \mathbf{k} + \mathbf{p} - \mathbf{q}, -\mathbf{k}, -\mathbf{p}) \times \\ & [A(\mathbf{k}, \mathbf{p}, -\mathbf{q}, -\mathbf{k} - \mathbf{p} + \mathbf{q}) + A(\mathbf{p}, \mathbf{k}, -\mathbf{q}, -\mathbf{k} - \mathbf{p} + \mathbf{q})]. \quad (25) \end{aligned}$$

$\Sigma(\mathbf{k}, \omega)$ is a sum over the ‘‘direct’’ and the ‘‘exchanged’’ diagrams; the factor of 4 is the multiplicity of each of these under rearranging the exterior lines. $\Sigma(\mathbf{k}, \omega)$ is seen to be $G_2(\mathbf{k}, \omega)$ with its incoming and outgoing lines removed.

The full interacting propagator $G(\mathbf{k}, \omega)$ can be approximated as a sum over repeated applications of ΣG_0 , i.e.,

$$G(\mathbf{k}, \omega) = G_0 + G_0(\Sigma G_0) + G_0(\Sigma G_0)^2 + \dots, \quad (26)$$

which, after summing, leads to the well-known Dyson equation,

$$G(\mathbf{k}, \omega) = \frac{1}{G_0^{-1} - \Sigma} = \frac{1}{\omega - \omega_{\mathbf{k}} + i\delta - \Sigma(\mathbf{k}, \omega)}. \quad (27)$$

The location of the pole gives the perturbed quasiparticle energy, $\omega'_{\mathbf{k}} = \omega_{\mathbf{k}} + \text{Re}\Sigma(\mathbf{k}, \omega_{\mathbf{k}})$, and the damping $\Gamma_{\mathbf{k}} = \Gamma(\mathbf{k}, \omega_{\mathbf{k}})$ is given by

$$\Gamma_{\mathbf{k}} = -\text{Im} \Sigma(\mathbf{k}, \omega_{\mathbf{k}}). \quad (28)$$

To apply the result to the system at finite temperature T , and obtain the self-energy associated with the temperature Green’s function, the integrals over frequency are transformed to sums according to

$$\int \frac{d\omega'}{2\pi} F(\omega') \rightarrow \frac{1}{\beta} \sum_{n=-\infty}^{\infty} F(i\omega_n), \quad (29)$$

$$\omega_n = \frac{2\pi}{\beta} n, \quad \beta = \frac{1}{k_B T}. \quad (30)$$

Thus the frequency integrals in (25) become

$$\begin{aligned} & \int \frac{d\omega'}{2\pi} \int \frac{d\omega''}{2\pi} G_0 G_0 G_0 \\ & \rightarrow - \frac{[n(\omega_{\mathbf{q}}) - n(-\omega_{\mathbf{k}+\mathbf{p}-\mathbf{q}})][n(\omega_{\mathbf{q}} + \omega_{\mathbf{k}+\mathbf{p}-\mathbf{q}}) - n(\omega_{\mathbf{p}})]}{\omega - (\omega_{\mathbf{k}+\mathbf{p}-\mathbf{q}} + \omega_{\mathbf{q}} - \omega_{\mathbf{p}})}, \quad (31) \end{aligned}$$

where the Bose factors are

$$n(\omega) = (e^{\beta\omega} - 1)^{-1} \approx 1/(\beta\omega). \quad (32)$$

The latter form applies to the classical limit. The imaginary part of Σ is derived from the analytic relation,

$$\frac{1}{x + i\delta} = P\left(\frac{1}{x}\right) - i\pi\delta(x), \quad (33)$$

where P takes the principal part and $\delta(x)$ is the usual delta-function. Because \mathbf{q} and \mathbf{p} each have two components, the sum in (25) is equivalent to a four-dimensional integration, once we take the continuum limit. Each dimension converts as, for example, $\sum_{q_x} \rightarrow \frac{L_x}{2\pi} \int dq_x$, where $L_x L_y = Na^2$ is the system size, in terms of the lattice constant a , leading to

$$\sum_{\mathbf{q}} \sum_{\mathbf{p}} \rightarrow \frac{N^2 a^2}{(2\pi)^4} \int_{-\pi}^{\pi} dq_x \int_{-\pi}^{\pi} dq_y \int_{-\pi}^{\pi} dp_x \int_{-\pi}^{\pi} dp_y. \quad (34)$$

The factors of N here are canceled by those in the expression for $A(\mathbf{q}_1, \mathbf{q}_2, \mathbf{q}_3, \mathbf{q}_4)$, leading to a size-independent result. Thus there finally results for the damping function,

$$\Gamma(\mathbf{k}, \omega) = \int d^2 q \int d^2 p F(\mathbf{q}, \mathbf{p}) \delta(\omega - \omega_{\mathbf{k}+\mathbf{p}-\mathbf{q}} + \omega_{\mathbf{p}} - \omega_{\mathbf{q}}), \quad (35)$$

where the kernel $F(\mathbf{q}, \mathbf{p})$ is given by

$$\begin{aligned} F(\mathbf{q}, \mathbf{p}) = & 4\pi \left(\frac{L}{2\pi}\right)^4 A(\mathbf{q}, \mathbf{k} + \mathbf{p} - \mathbf{q}, -\mathbf{k}, -\mathbf{p}) \times \\ & [A(\mathbf{p}, \mathbf{k}, -\mathbf{q}, -\mathbf{k} - \mathbf{p} + \mathbf{q}) + A(\mathbf{k}, \mathbf{p}, -\mathbf{q}, -\mathbf{k} - \mathbf{p} + \mathbf{q})] \times \\ & [n(\omega_{\mathbf{q}}) - n(-\omega_{\mathbf{k}+\mathbf{p}-\mathbf{q}})][n(\omega_{\mathbf{q}} + \omega_{\mathbf{k}+\mathbf{p}-\mathbf{q}}) - n(\omega_{\mathbf{p}})]. \quad (36) \end{aligned}$$

We use this result to calculate the damping at the spin-wave frequency: $\Gamma_{\mathbf{k}} = \Gamma(\mathbf{k}, \omega = \omega_{\mathbf{k}})$, in the thermodynamic limit $L \rightarrow \infty$. Note that in the classical limit, the Bose factors are simply proportional to temperature. Therefore, we only need to calculate $\Gamma_{\mathbf{k}}$ at one temperature ($T = 1.0J$) and then scale with T^2 to get its value at other temperatures.

A. Evaluation of contour integrals in four dimensions

The summation/integration in (35) involving a delta function presents an interesting mathematical problem in its evaluation. General integrals of this form (i.e., with one delta-function) in d dimensions can be considered,

$$D(\omega) = \int d^d x f(\mathbf{x}) \delta(\omega - g(\mathbf{x})), \quad (37)$$

where \mathbf{x} is a d -dimensional vector. In two dimensions, for example, the delta-function will pick off a particular contour that contributes to the integral; in three dimensions that contour will actually be a surface, and in four dimensions it will be a three-dimensional volume. Depending on the form of the function $g(\mathbf{x})$, the contributing region need not be simply connected, but may consist of separated distinct parts. For the higher dimensional cases, it is difficult to visualize the region or regions that contribute to the integral. Thus it is necessary to have a way to evaluate the integral without appealing directly to geometrical properties.

In a series of papers, Gilat and co-workers^{9–11} have considered how to evaluate these integrals in three dimensions, in work related the calculation of spectral density functions. We have used the “linear analytic” (LA) method¹⁰ of Gilat and Raubenheimer, extended to four dimensions, which gives good precision for few sample points, at little cost in complexity. Suppose we calculate $D(\omega)$ over a small range of ω and then take the limit $\omega \rightarrow \omega_{\mathbf{k}}$. To do so, a 4D cubic grid of small cells of size $(2b)^4$ is set in the \mathbf{x} -space. Then we consider the contribution of each cell to $D(\omega)$, thereafter summing over the cells. Suppose the cells are small enough so that the kernel $f(\mathbf{x})$ has only a small variation within a cell, and, therefore, we can use its value at the cell center, \mathbf{x}_c . Then we can write

$$D(\omega) = \sum_{\text{cells}} D_{\text{cell}}(\omega), \quad (38)$$

$$D_{\text{cell}}(\omega) = f(\mathbf{x}_c) \int_{\text{cell}} d^4 x \delta(\omega - g(\mathbf{x})). \quad (39)$$

The idea of the LA method is to expand $g(\mathbf{x})$ around the cell center,

$$g(\mathbf{x}) \approx g(\mathbf{x}_c) + (\mathbf{x} - \mathbf{x}_c) \cdot \nabla g(\mathbf{x}_c). \quad (40)$$

Shifting coordinates to $\mathbf{u} = \mathbf{x} - \mathbf{x}_c$, and writing the gradient at the cell center as $\nabla g(\mathbf{x}_c) = |\nabla g(\mathbf{x}_c)| \hat{\mathbf{l}}$, where the unit vector $\hat{\mathbf{l}} = (l_1, l_2, l_3, l_4)$ points along the gradient evaluated at the cell center, we have

$$D_{\text{cell}}(\omega) = \frac{f(\mathbf{x}_c)}{|\nabla g(\mathbf{x}_c)|} \int_{\text{cell}} d^4 u \delta(w - \mathbf{u} \cdot \hat{\mathbf{l}}), \quad (41)$$

$$w = \frac{\omega - g(\mathbf{x}_c)}{|\nabla g(\mathbf{x}_c)|}. \quad (42)$$

The variable w is a rescaling of ω . If we use the integral representation of the delta function, in the form,

$$\delta(w - \mathbf{u} \cdot \hat{\mathbf{l}}) = \frac{1}{2\pi} \int_{-\infty}^{\infty} dk e^{ik(w - u_1 l_1 - u_2 l_2 - u_3 l_3 - u_4 l_4)}, \quad (43)$$

then the contribution from one cell is found to be

$$\begin{aligned} D_{\text{cell}}(\omega) &= \frac{f(\mathbf{x}_c)}{|\nabla g(\mathbf{x}_c)|} \frac{1}{2\pi} \int_{-\infty}^{\infty} dk e^{ikw} \prod_{j=1}^4 \int_{-b}^b du_j e^{-iku_j l_j} \\ &= \frac{f(\mathbf{x}_c)}{|\nabla g(\mathbf{x}_c)|} \frac{1}{12|l_1 l_2 l_3 l_4|} \sum_{i=1}^{16} (-1)^{m_i} |w + w_i|^3, \end{aligned} \quad (44)$$

where the w_i are the values of parameter w at the 16 corners of the cell, i.e.,

$$w_i = b(\pm l_1 \pm l_2 \pm l_3 \pm l_4), \quad (45)$$

with all 16 possible choices of the signs, and m_i is the number of minus signs used in each w_i . One can note that similar simple formulas result for this type of integral in other dimensions as well.¹²

In the actual application of Eq. (44), inside the cell, the parameter w will range between minimum and maximum values:

$$w_{\text{max}} = b(|l_1| + |l_2| + |l_3| + |l_4|) = -w_{\text{min}}. \quad (46)$$

These values hold at two opposite corners of the cell. By Eq. (42), there will be a corresponding range of ω over which this cell contributes to $D(\omega)$. Then for the general problem where D is desired over a large range of ω , what is done is to set a uniform grid of ω -values, finding the contribution of each cell to $D(\omega)$ for each value on the grid, say, $\omega = \omega_n$. Typically it works well to have the grid fine enough so that each cell contributes to D at many different ω_n .

B. Numerical calculation of $\Gamma_{\mathbf{k}}$

For the damping problem, Eq. (35), we have the replacements,

$$f(\mathbf{x}) = F(\mathbf{q}, \mathbf{p}), \quad g(\mathbf{x}) = \omega_{\mathbf{k}+\mathbf{p}-\mathbf{q}} - \omega_{\mathbf{p}} + \omega_{\mathbf{q}}, \quad (47)$$

with the 4D variable $\mathbf{x} = (\mathbf{q}, \mathbf{p})$. We want to find $\Gamma(\mathbf{k}, \omega)$ right at $\omega = \omega_{\mathbf{k}}$ for some particular wavevector, \mathbf{k} . To accomplish this, we set a range $\omega_{\min} \leq \omega \leq \omega_{\max}$, and define the grid of values $\omega_n = \omega_{\min} + n(\omega_{\max} - \omega_{\min})/N_{\text{grid}}$, using $N_{\text{grid}} = 500$. For the integrations over \mathbf{q} and \mathbf{p} , the cell sizes actually can be quite large: we used the cell width $2b = 2\pi/L$, where $L = 41$ is a “system size,” which gave results consistent with those using much smaller cells (larger L). That is, each axis, q_x, q_y, p_x, p_y , was partitioned into 41 cells. First, to get good precision, a narrow range symmetrical around the spinwave frequency was used: $\omega_{\min} = \omega_{\mathbf{k}} - 0.1JS$, $\omega_{\max} = \omega_{\mathbf{k}} + 0.1JS$. Second, for comparison, the behavior of the damping function was calculated over the whole range of possible spinwave frequencies, i.e., $\omega_{\min} = 0$, $\omega_{\max} \approx \omega_{\mathbf{q}=(\pi,\pi)} = 4\sqrt{2(1+\lambda)}JS$. In both of these approaches, interpolation on the ω -grid gives $\Gamma(\mathbf{k}, \omega_{\mathbf{k}})$. The scheme was found to be very robust, with both approaches agreeing to better than one percent precision.

We should also note one other important calculational detail. Because Eq. (44) depends on the reciprocal gradient of g , it is necessary to avoid any points in the \mathbf{q}, \mathbf{p} -space where this gradient vanishes. We accomplished this by taking wavevectors $\mathbf{k} = (x_k, y_k)\frac{2\pi}{L}$, (at $L = 41$), and then shifting the \mathbf{q}, \mathbf{p} -cell center positions slightly from the usual values: $\mathbf{q} = (x_q + \frac{1}{2}, y_q + \frac{1}{2})\frac{2\pi}{L} + (\Delta, \Delta)$, $\mathbf{p} = (x_p + \frac{1}{2}, y_p + \frac{1}{2})\frac{2\pi}{L} + (\Delta, \Delta)$. Here x_k, y_k, x_q, y_q , etc., are integers ranging from 0 to $L - 1$, and we used $\Delta = 0.022378$ to shift the \mathbf{q}, \mathbf{p} -cells away from high symmetry points. The choice of an odd number for L also helps to avoid certain high symmetry points. Some slight improvement in precision can be achieved with a larger value of L , however, at the expense of a tremendous increase in cpu time, which varies as 4^L . At $L = 41$, the typical relative errors in $\Gamma(\mathbf{k}, \omega)$ were found to be much less than one percent, when compared to calculations using $L = 81$.

Some results for the damping function, which is proportional to T^2 , are shown in Fig. 3 for $\lambda = 0$. In general, it is found that $\Gamma(\mathbf{k}, \omega)$ either has a cusp or a peak at the spinwave frequency (arrows in Fig. 3). The damping strength increases with $|\mathbf{k}|$, as seen in Fig. 4. Along the (11) direction, however, $\Gamma_{\mathbf{k}}$ tends to saturate halfway out in the zone. Keeping in mind that $\Gamma_{\mathbf{k}} \propto T^2$, the damping strength we find here is quite weak, especially when we consider its effects at $T \ll J$ where the spinwave approximation is valid.

At small nonzero values of the anisotropy parameter λ , there will be only a very slight change in $\Gamma_{\mathbf{k}}$, because λ does not appear explicitly in H_1 , but only enters the calculation via the dispersion relation and via the α and β functions of (13). To demonstrate this effect, Fig. 5 shows $\Gamma_{\mathbf{k}}$ at various values of λ for k along the (10) direction. In general, the damping decreases with increasing λ , i.e. as the system becomes more isotropic.

The calculation of the memory function requires the knowledge of $\Gamma_{\mathbf{k}}$ over the entire BZ. We can reduce the

region of calculation to $k_x \geq k_y \geq 0$, because, by symmetry, $\Gamma_{\mathbf{k}} = \Gamma_{-\mathbf{k}}$, and $\Gamma_{(k_x, k_y)} = \Gamma_{(k_y, k_x)}$. In this region $\Gamma_{\mathbf{k}}$ was calculated on a uniform square grid with spacing $\Delta k_x = \Delta k_y = 2\pi/50$. Linear interpolation was used to get values between these grid points.

IV. THE MEMORY FUNCTION FORMALISM WITH DAMPING

For the calculation of the dynamic correlation function $S(q, \omega)$, we use the memory function formalism due to Reiter and Sjölander,¹³ who applied the procedure to the isotropic Heisenberg model. The technique is based on a low-temperature expansion of the memory function.¹⁴ The formalism was applied to the 1D isotropic antiferromagnet in an external field by De Raedt et al¹⁵ and to a 1D easy-plane antiferromagnet by Gouvêa and Pires.¹⁶ More recently, it was also applied to 2D easy-plane ferromagnets by Menezes et al,¹⁷ although some numerical difficulties inhibited numerical evaluation of the analytic formulas. Some of these problems were surpassed in the work of Pereira et al.^{18,19} In all of these works, no mode damping was included. The presence of damping actually relieves the numerical difficulty of the problem, as we see below.

The dynamic correlation function is defined in terms of the Fourier transformed spin-fields as

$$S^{\alpha\alpha}(\mathbf{q}, \omega) = \frac{1}{2\pi} \int_{-\infty}^{\infty} dt e^{-i\omega t} \langle S^{\alpha}(\mathbf{q}, t) S^{\alpha}(-\mathbf{q}, 0) \rangle, \quad (48)$$

where α is any component of S , and by symmetry, $S^{xx}(\mathbf{q}, \omega) = S^{yy}(\mathbf{q}, \omega)$. In this and following formulas for correlation functions, we note the distinction between continuum (functions of \mathbf{q}) and discrete (subscripts \mathbf{q}) Fourier transforms, which are related by factors of $2\pi/L$ for each dimension.²⁰ This is necessary so that we can make a careful comparison between the theory and the MC-SD simulations, *including the absolute magnitudes*. Specifically, the continuum correlation function in (48), which gives a thermodynamic weight over a *wavevector range* $d^2q = (2\pi/L)^2$, is related to the discrete correlation at a *specific* wavevector \mathbf{q} , using discrete Fourier transforms as defined in (9), by²¹

$$\langle S^{\alpha}(\mathbf{q}, t) S^{\alpha}(-\mathbf{q}, 0) \rangle = \frac{1}{(2\pi)^2} \langle S_{\mathbf{q}}^{\alpha}(t) S_{-\mathbf{q}}^{\alpha}(0) \rangle. \quad (49)$$

In the analytic calculations, many intermediate quantities are discrete functions, however, for the comparison with the MC-SD data, both results will be converted and displayed as continuum quantities.

Due to the symmetry in the xy -plane, the calculation is carried out by making averages of the rotationally symmetric quantity, $S_{\mathbf{q}}^{\perp} = S_{\mathbf{q}}^x + S_{\mathbf{q}}^y$, with $S^{xx}(\mathbf{q}, \omega) = \frac{1}{2} S^{\perp\perp}(\mathbf{q}, \omega)$. Then in the memory function calculation,

the continuum dynamical structure function can be written in terms of a second-order memory function, $\Sigma_{\mathbf{q}}^{\perp}(\omega)$, to be described below, according to

$$S^{\perp\perp}(\mathbf{q}, \omega) = \frac{(2\pi)^{-2} \pi^{-1} \langle LS_{\mathbf{q}}^{\perp}, LS_{-\mathbf{q}}^{\perp} \rangle \text{Im } \Sigma_{\mathbf{q}}^{\perp}(\omega)}{[\omega^2 - \langle \omega^2 \rangle_{\mathbf{q}}^{\perp} + \omega \text{Re } \Sigma_{\mathbf{q}}^{\perp}(\omega)]^2 + [\omega \text{Im } \Sigma_{\mathbf{q}}^{\perp}(\omega)]^2}, \quad (50)$$

where $L = -i d/dt$ is the Liouville operator, and the second moment $\langle \omega^2 \rangle_{\mathbf{q}}^{\perp}$ is determined from a ratio,

$$\langle \omega^2 \rangle_{\mathbf{q}}^{\perp} = \frac{\langle S_{\mathbf{q}}^{\perp}, LS_{\mathbf{q}}^{\perp} \rangle}{\langle S_{\mathbf{q}}^{\perp}, S_{-\mathbf{q}}^{\perp} \rangle}. \quad (51)$$

The location of the spinwave peak that results from Eq. (50) is very sensitive to the value of $\langle \omega^2 \rangle_{\mathbf{q}}^{\perp}$, therefore we are especially concerned to get an accurate evaluation of it. The denominator of (51) is a static correlation function, whose value will be taken from the Monte Carlo simulations, although for low temperatures it can be evaluated approximately as

$$\langle S_{\mathbf{q}}^{\perp} S_{-\mathbf{q}}^{\perp} \rangle \approx (1 - \langle z_{\mathbf{n}}^2 \rangle) \frac{T}{4J} (1 - \gamma_{\mathbf{q}})^{-1}, \quad (52a)$$

$$\langle z_{\mathbf{n}}^2 \rangle \approx \frac{T}{4J}, \quad (52b)$$

The numerator of (51) has been shown^{17,18} to have a leading low-temperature dependence, also related to static nearest neighbor correlations,

$$\langle LS_{\mathbf{q}}^{\perp}, LS_{-\mathbf{q}}^{\perp} \rangle = 4JT(1 - \lambda\gamma_{\mathbf{q}}) \langle S_{a\hat{x}}^{\perp} S_0^{\perp} \rangle - 8JT(\gamma_{\mathbf{q}} - \lambda) \langle S_{a\hat{x}}^z S_0^z \rangle. \quad (53)$$

The correlation $\langle S_{a\hat{x}}^z S_0^z \rangle \propto \lambda T$, therefore its contribution can be ignored for small λ . There being two bonds per lattice site, the in-plane near-neighbor correlation is related to the average energy per bond by

$$\left\langle \frac{E}{2JN} \right\rangle = S^2 - \langle \vec{S}_{a\hat{x}} \cdot \vec{S}_0 \rangle \approx S^2 - \langle S_{a\hat{x}}^{\perp} S_0^{\perp} \rangle. \quad (54)$$

This correlation can also be obtained from the MC simulations, although a good low-T approximation is

$$\langle S_{a\hat{x}}^{\perp} S_0^{\perp} \rangle \approx \left(1 - \frac{T}{4J}\right) e^{-1.273 \frac{T}{4J}}. \quad (55)$$

A comparison of the analytic and MC static parameters will be given below.

To the leading order in temperature, the time-dependent memory function has been shown to be given from

$$\Sigma_{\mathbf{q}}^{\alpha}(t) = -\langle LS_{\mathbf{q}}^{\alpha} LS_{-\mathbf{q}}^{\alpha} \rangle^{-1} M_{\mathbf{q}}^{\alpha}(t), \quad (56a)$$

$$M_{\mathbf{q}}^{\alpha}(t) = \langle QL^2 S_{\mathbf{q}}^{\alpha} e^{-iLt} QL^2 S_{-\mathbf{q}}^{\alpha} \rangle, \quad (56b)$$

where Q is projection onto the non-secular variables, see Ref. 13, whose action is equivalent to

$$QL^2 S_{\mathbf{q}}^{\alpha} = (L^2 - \langle \omega^2 \rangle_{\mathbf{q}}^{\alpha}) S_{\mathbf{q}}^{\alpha}. \quad (57)$$

Using expressions (4) expanded to second order in $\phi_{\mathbf{n}}$, $z_{\mathbf{n}}$, and (13), it is straightforward to write the spins $S_{\mathbf{n}}$ in terms of the creation/annihilation operators. In the leading order in temperature, the resulting expressions involve expectation values of products of four creation/annihilation operators. The damping is included in the time evolution according to,

$$a_{\mathbf{q}}^{\dagger}(t) = a_{\mathbf{q}}^{\dagger}(0) e^{(i\omega - \Gamma_{\mathbf{q}})t}, \quad a_{\mathbf{q}}(t) = a_{\mathbf{q}}(0) e^{(-i\omega - \Gamma_{\mathbf{q}})t}. \quad (58)$$

Then, there results, after some manipulations, expressions to give the memory function,

$$M_{\mathbf{q}}^{\perp}(t) = \frac{1}{N} \sum_{\mathbf{p}} \left\{ W_{+}(\mathbf{q}, \mathbf{p}) e^{-\Gamma_{+}(\mathbf{q}, \mathbf{p})t} \cos \Omega_{+}(\mathbf{q}, \mathbf{p})t + W_{-}(\mathbf{q}, \mathbf{p}) e^{-\Gamma_{-}(\mathbf{q}, \mathbf{p})t} \cos \Omega_{-}(\mathbf{q}, \mathbf{p})t \right\}. \quad (59)$$

The two terms correspond to spinwave sum (Ω_{+}) and difference (Ω_{-}) processes, with weights

$$W_{\pm}(\mathbf{q}, \mathbf{p}) = n(\omega_{\frac{\mathbf{q}}{2} + \mathbf{p}}) n(\omega_{\frac{\mathbf{q}}{2} - \mathbf{p}}) (\tilde{s} \mp \tilde{t})^2, \quad (60)$$

where

$$\tilde{s} = S \beta_{\frac{\mathbf{q}}{2} + \mathbf{p}} \beta_{\frac{\mathbf{q}}{2} - \mathbf{p}} \left\{ \omega_{\mathbf{q}}^2 - (4JS)^2 \times \left[(1 - \gamma_{\frac{\mathbf{q}}{2} + \mathbf{p}}) (\gamma_{\frac{\mathbf{q}}{2} - \mathbf{p}} - \lambda \gamma_{\frac{\mathbf{q}}{2} + \mathbf{p}}) + (1 - \gamma_{\frac{\mathbf{q}}{2} - \mathbf{p}}) (\gamma_{\frac{\mathbf{q}}{2} + \mathbf{p}} - \lambda \gamma_{\frac{\mathbf{q}}{2} - \mathbf{p}}) \right] \right\}, \quad (61a)$$

$$\tilde{t} = S \alpha_{\frac{\mathbf{q}}{2} + \mathbf{p}} \alpha_{\frac{\mathbf{q}}{2} - \mathbf{p}} \left\{ \omega_{\mathbf{q}}^2 + (4JS)^2 \times \left[(1 - \lambda \gamma_{\frac{\mathbf{q}}{2} - \mathbf{p}}) (\gamma_{\frac{\mathbf{q}}{2} - \mathbf{p}} - \lambda \gamma_{\frac{\mathbf{q}}{2} + \mathbf{p}}) + (1 - \lambda \gamma_{\frac{\mathbf{q}}{2} + \mathbf{p}}) (\gamma_{\frac{\mathbf{q}}{2} + \mathbf{p}} - \lambda \gamma_{\frac{\mathbf{q}}{2} - \mathbf{p}}) \right] \right\}. \quad (61b)$$

The frequencies and damping rates of these processes are

$$\Omega_{\pm}(\mathbf{q}, \mathbf{p}) = \omega_{\frac{\mathbf{q}}{2} + \mathbf{p}} \pm \omega_{\frac{\mathbf{q}}{2} - \mathbf{p}}, \quad (62a)$$

$$\Gamma_{\pm}(\mathbf{q}, \mathbf{p}) = \Gamma_{\frac{\mathbf{q}}{2} + \mathbf{p}} + \Gamma_{\frac{\mathbf{q}}{2} - \mathbf{p}}. \quad (62b)$$

Finally, the frequency-dependent memory function is given by the one-sided Fourier-Laplace transform,

$$\Sigma_{\mathbf{q}}^{\perp}(\omega) = -i \int_0^{\infty} dt e^{i\omega t} \Sigma_{\mathbf{q}}^{\perp}(t). \quad (63)$$

From this expression, Eq. (59), and equations following, we obtain a sum over all the sum/difference processes,

$$\Sigma_{\mathbf{q}}^{\perp}(\omega) = \frac{-1}{2N} \langle LS_{\mathbf{q}}^{\perp} LS_{-\mathbf{q}}^{\perp} \rangle^{-1} \sum_{\mathbf{p}} \left\{ W_{+} \left[\frac{\omega + \Omega_{+} - i\Gamma_{+}}{(\omega + \Omega_{+})^2 + \Gamma_{+}^2} + \frac{\omega - \Omega_{+} - i\Gamma_{+}}{(\omega - \Omega_{+})^2 + \Gamma_{+}^2} \right] + W_{-} \left[\frac{\omega + \Omega_{-} - i\Gamma_{-}}{(\omega + \Omega_{-})^2 + \Gamma_{-}^2} + \frac{\omega - \Omega_{-} - i\Gamma_{-}}{(\omega - \Omega_{-})^2 + \Gamma_{-}^2} \right] \right\}. \quad (64)$$

where the (\mathbf{q}, \mathbf{p}) dependencies of W_{\pm}, Ω_{\pm} , and Γ_{\pm} have been suppressed. This is the expression used to evaluate $\Sigma_{\mathbf{q}}^{\perp}$, and thus the dynamic structure function, via Eq. (50).

To evaluate (64) on a discrete $L \times L$ lattice, the wavevector \mathbf{q} must be one of the allowed values,

$$\mathbf{q} = (x_q, y_q)(2\pi/L), \quad (65)$$

where x_q and y_q are integers. It is also necessary to make the summations over \mathbf{p} such that the vectors $\frac{\mathbf{q}}{2} \pm \mathbf{p}$ are both given by integers times $2\pi/L$. Thus, it is convenient to change from the summation over \mathbf{p} to a summation over a new variable \mathbf{k} defined by

$$\mathbf{k} \equiv \frac{\mathbf{q}}{2} + \mathbf{p} = (x_k, y_k)(2\pi/L), \quad (66)$$

where x_k and y_k are integers. Then, we also have $\frac{\mathbf{q}}{2} - \mathbf{p} = \mathbf{q} - \mathbf{k}$ equal to an allowed wavevector. This insures that the sums will be over spinwaves that are allowed on the given finite lattice. This approach is essential for calculation of the finite size dynamical effects. On the other hand, for the infinite sized system, no variable change is needed, and there is the usual replacement, $\frac{1}{N} \sum_{\mathbf{p}} \rightarrow (2\pi)^{-2} \int d^2p$.

Note that in the limit of zero damping, Eq. (64) is inapplicable, except for the continuum limit (i.e., $L \rightarrow \infty$). The resulting continuum integrals for the infinite system are singular, and the analytic relation (33) must be applied, leading to

$$\Sigma_{\mathbf{q}}^{\perp}(\omega) = \frac{1}{2(2\pi)^2} \langle LS_{\mathbf{q}}^{\perp} LS_{-\mathbf{q}}^{\perp} \rangle^{-1} \times \left\{ P \int d^2p W_{+} \left[\frac{1}{\omega + \Omega_{+}} + \frac{1}{\omega - \Omega_{+}} \right] + P \int d^2p W_{-} \left[\frac{1}{\omega + \Omega_{-}} + \frac{1}{\omega - \Omega_{-}} \right] - i\pi \int d^2p W_{+} \left[\delta(\omega + \Omega_{+}) + \delta(\omega - \Omega_{+}) \right] - i\pi \int d^2p W_{-} \left[\delta(\omega + \Omega_{-}) + \delta(\omega - \Omega_{-}) \right] \right\}. \quad (67)$$

Indeed, in the very low temperature range ($T < 0.2J$) where the damping is extremely weak, it may be more efficient to use this expression rather than Eq. (64), which has poorer convergence with L . Eq. (67) was applied by Pereira et al.^{18,19}; the imaginary part can be evaluated by techniques described here (Sec. III A), and the principal-valued real part can be calculated by an extension²² of

techniques used in 1D.²³ In Ref. 19 the last expression was found to give finite amplitude spinwave peaks, without damping present.

Before presenting the results obtained via the memory function approach, the key aspects of the Monte Carlo and spin-dynamics simulations are summarized.

V. MONTE CARLO AND SPIN-DYNAMICS

To test the validity of the memory function technique, we compare it with numerical simulations on $L \times L$ square lattices ($L = 128$, $\lambda = 0$) using Monte-Carlo and spin-dynamics (SD) simulations, which include effects due to all thermodynamically allowed excitations. As mentioned above, we also use some data for static correlations from the Monte Carlo calculations as input to the memory function dynamical calculations. The techniques used here have been described in Ref. 24 and are based on the simulation methods developed in Ref. 25.

In the MC calculation, we applied a combination of Metropolis single-spin moves and over-relaxation moves that modify all three spin components, and in addition, Wolff single-cluster operations²⁶ that modify *only* the xy spin components. The over-relaxation and cluster moves are important at low temperatures, where the xy spin components tend to freeze and single spin moves become inefficient.

In the combined MC-SD simulations, a set of MC generated states from thermodynamic equilibrium at temperature T are used as initial conditions for numerical integrations in time via a fourth order Runge-Kutta scheme. Specifically, the first 4000 MC steps were used for equilibrating the system. Then, every 400 MC steps a state was taken to initiate the SD integration. This was repeated 500 times; the displayed $S(\mathbf{q}, \omega)$ data are averages over the 500 time integrations. The total MC sequence was then 2×10^5 steps; every 25 steps a state was used to calculate averages of the static correlation functions.

In the time integration, the basic Runge-Kutta time step was $\Delta t = 0.03(JS)^{-1}$, and every 11 time steps, data samples (for $S_{\mathbf{q}}^x(t)$, etc.) were saved for \mathbf{q} 's in the (10), (01), and (11) directions only (due to machine memory restrictions). A total of 2^{12} data samples were saved, followed by applying a fast-Fourier-transform to obtain $S^{xx}(\mathbf{q}, \omega)$. The total time of integration of $t_{\max} = 1351.68(JS)^{-1}$ is large enough so that no smoothing window is necessary for the data generation. Then the frequency resolution of these results is good, $\Delta\omega = 2\pi/t_{\max} = 0.0046484JS$, so that any fine details in the low temperature results should be visible. For the lowest temperatures ($T \leq 0.3J$), where we wanted to see the complex fine details due to the finite size effects, some simulations were made saving data samples every 28 times steps, leading to a total integration time $t_{\max} = 3440.64(JS)^{-1}$, and frequency resolu-

tion $\Delta\omega = 2\pi/t_{\max} = 0.0018262JS$.

VI. NUMERICAL RESULTS

First, a comparison of the low- T formulas and static MC results needed as input to the memory function formalism is presented. Then dynamical results from the memory function and from MD-SD will be presented for large systems, and finally, for smaller systems, where the finite size features will be analyzed.

A. Statics

The continuum static structure function,

$$S^{xx}(\mathbf{q}) = \frac{1}{2(2\pi)^2} \langle S_{\mathbf{q}}^{\perp} S_{-\mathbf{q}}^{\perp} \rangle, \quad (68)$$

was measured directly in the MC simulations. A comparison with the results based on the low-temperature expression (52) is given in Fig. 6. There we also show a fit of the MC data to a form similar to the analytic expression, but with a fitting coefficient (A) and power (B),

$$\langle S_{\mathbf{q}}^{\perp} S_{-\mathbf{q}}^{\perp} \rangle_{\text{fitted}} = A(1 - \gamma_{\mathbf{q}})^{-B}. \quad (69)$$

From the fits, the parameter A is somewhat larger than the low-temperature limit, $A = T/(4J)$. This can be expected due to the renormalization of the effective J to lower values with temperature. The power B falls with increasing T , which must also be due to anharmonic effects. There is little difference between the low- T expression and the MC data at the lowest temperature. The deviations between the MC and low- T theory increase substantially by $T = 0.5J$, especially at higher wavevectors. Note that the fits are only shown for demonstration; we used the MC data itself as inputs to the memory function calculations.

The other static input to the memory function calculation, for determining the second moment, is the quantity $\langle LS_{\mathbf{q}}^{\perp} LS_{-\mathbf{q}}^{\perp} \rangle$, which is related to the nearest neighbor correlation $\langle S_{ax}^{\perp} S_{0}^{\perp} \rangle$ by Eq. (53). Estimates of that latter from the MC evaluation of the average energy per spin [Eq. (54)] are compared to the theoretical expression (55) in Fig. 7. The analytical expression is seen to give results consistent with the MC data up to $T \approx 0.5J$.

When combined to give the second moment, the MC data produces results as shown in Fig. 8. It is essentially this quantity that has the strongest influence on the locations of the spinwave peaks in $S(\mathbf{q}, \omega)$. These are the data used as input to the memory function calculation.

B. Dynamics: Memory Function compared with MC-SD

We evaluate $\Sigma_{\mathbf{q}}^{\perp}(\omega)$ by using the sum over discrete wavevectors \mathbf{p} as displayed in Eq. (64), and then apply Eq. (50) to determine $S^{xx}(\mathbf{q}, \omega) = \frac{1}{2} S^{\perp\perp}(\mathbf{q}, \omega)$. If L is taken large enough, then the sum should be a good approximation to the infinite size limit. In general, we can see whether larger L is necessary by the presence of finite size features in the data for $\Sigma_{\mathbf{q}}^{\perp}$ and $S^{xx}(\mathbf{q}, \omega)$. Typically we used $L = 1024$ to give a reasonable approximation to the continuum limit for $T \geq 0.3J$ and larger \mathbf{q} -values; at lower temperatures or wavevectors even larger L is necessary to smooth out all the finite size features, due to the very weak damping.

In Fig. 9, some typical results for the real and imaginary parts of $\Sigma_{\mathbf{q}}^{\perp}(\omega)$ are shown for $\lambda = 0$, $T = 0.3J$, and $\mathbf{q} = (\pi/4, \pi/4)$, where $L = 2048$ was used in the sum. The resulting dynamical structure function is compared to the corresponding MC-SD data for $L = 128$ in Fig. 10. At the (zero- T) spinwave frequency $\omega_{\mathbf{q}} = 2.16478JS$, $\text{Im} \Sigma_{\mathbf{q}}^{\perp}(\omega)$ achieves its minimum value, which is not zero due to the presence of the damping, while $\text{Re} \Sigma_{\mathbf{q}}^{\perp}(\omega)$ has a small nonzero value there as well. The spinwave peak in the memory data occurs at $\omega = \omega_{\text{peak}} = 2.005JS$, which is just slightly greater than the associated value of the second moment, $\omega_{\mathbf{q}}^{\perp} \equiv \sqrt{\langle \omega^2 \rangle_{\mathbf{q}}^{\perp}} = 1.9648JS$. The spinwave peak position will occur where the denominator of Eq. (50) achieves its minimum value, which gives, to a good approximation,

$$\omega_{\text{peak}} = \omega_{\mathbf{q}}^{\perp} \sqrt{1 - \text{Re} \Sigma_{\mathbf{q}}^{\perp}(\omega_{\mathbf{q}}^{\perp}) / \omega_{\mathbf{q}}^{\perp}}. \quad (70)$$

For this case, the memory function data give $\text{Re} \Sigma_{\mathbf{q}}^{\perp}(\omega_{\mathbf{q}}^{\perp}) \approx -0.081JS$, which is consistent with this relation. The peak position is very sensitive to the value of the second moment, which is why we have tried to estimate it as accurately as possible from the static MC data. Still, the MC-SD data show the spinwave peak closer to $\omega = 1.98JS$, slightly lower than the memory function prediction. Using Eq. (50), the spinwave peak height is proportional to $[\text{Im} \Sigma(\omega_{\text{peak}})]^{-1}$, while the peak width is approximately equal to $\text{Im} \Sigma(\omega_{\text{peak}})$. When compared to the MC-SD data, the memory function calculation usually overestimates the peak height and underestimates the peak width, although both are in reasonable agreement with the MC-SD data. In fact, these errors tend to be larger at lower temperature.

In Figs. 11–13, we display some further comparisons of the memory function calculations and MC-SD results at other values of \mathbf{q} for temperatures ranging from $T = 0.1J$ to $T = 0.5J$. For the lower temperatures there is very good agreement between the memory theory and MC-SD peak positions, while the peak heights and widths do not agree as well. On the other hand, at higher temperatures the opposite is true: the memory data show greater errors in the peak positions, especially at large

q , but the peak heights and widths are predicted very well. Probably these discrepancies are caused by a fairly large *underestimate* of the damping strength at low temperature, as well as errors in the estimate of the second moment at higher temperatures. However, in general, the tails of the spinwave peaks far from $\omega_{\mathbf{q}}$ are described very well by the memory function calculations.

C. Dynamics: Small Systems and Finite Size Effects

When we consider the results using relatively smaller values of wavevector, $S^{xx}(\mathbf{q}, \omega)$ shows not only a spinwave peak, but additional features (small peaks) which depend on the system size. These features are obvious in the MC-SD $S(\mathbf{q}, \omega)$ data shown above. Similar size-dependent dynamical features have been noticed in earlier MC-SD simulations of XY-symmetry^{24,27,28} and easy-axis symmetry²⁹ magnets, but without a clear theoretical explanation. We now consider a closer look at the details of these features, making a comparison with the memory function calculations at smaller values of L .

Some examples showing the resulting memory function data for $S^{xx}(\mathbf{q}, \omega)$ for $L = 128$ systems are given in Fig. 14a [$\mathbf{q} = (16, 0)2\pi/L$, $T = 0.3J$], Fig. 15a [$\mathbf{q} = (9, 0)2\pi/L$, $T = 0.3J$], and Fig. 16a [$\mathbf{q} = (5, 0)2\pi/L$, $T = 0.1J$]. In fact, there appear various sequences of small peaks. The number of separate sequences appears to depend on the wavevector in integer units of $2\pi/L$. Note that the logarithmic scale exaggerates the size of these subpeaks, they are typically a few orders of magnitude smaller than the spinwave peak. For sufficiently low temperatures, these effects also appear clearly in the MC-SD results: see Figs. 14b, 15b and 16b, although the corresponding features there are smeared out compared to the memory function calculation. The effects are also present at larger wavevectors, however, in that case there are many more of these finite size subpeaks, which tend to merge together into a smoother background.

These extra peaks can each be associated with particular spinwave sum or difference process. To see that this is the case, consider first the difference processes, whose frequencies $\Omega_-(\mathbf{q}, \mathbf{p})$ are always less than the spinwave frequency $\omega_{\mathbf{q}}$. A plot of the weights W_- [Eq. (60)] that determine the contributions to the memory function versus the corresponding frequencies $\Omega_- = \omega_{\mathbf{k}} - \omega_{\mathbf{q}-\mathbf{k}}$, can show how strongly each process [i.e., each \mathbf{k} as defined in (66)] contributes to $\text{Im} \Sigma_{\mathbf{q}}^{\perp}$ and hence to $S(\mathbf{q}, \omega)$. In Fig. 17, we made such a plot for an even integer \mathbf{q} , namely, $\mathbf{q} = (16, 0)2\pi/L$, for $L = 128$ and $T = 0.3J$. Each dot there corresponds to one allowed wavevector \mathbf{k} ; some of the values of \mathbf{k} in units of $2\pi/L$ are indicated there. The sequence of \mathbf{k} 's, (8,0), (8,1), (8,2), etc., leads to multiple contributions at zero frequency, that is, a weak central peak, which is a general result for any even integer \mathbf{q} . The sequence, (9,0), (9,1), (9,2), etc., produces a sequence of small peaks in $S(\mathbf{q}, \omega)$ out to $\omega \approx 0.2JS$, and,

the next sequence, (10,0), (10,1), (10,2), etc., gives a sequence of peaks out to $\omega \approx 0.4JS$, and so on. Each of these \mathbf{k} -sequences can be identified with corresponding peak-sequences in the memory function calculation of $S(\mathbf{q}, \omega)$, as seen in Fig. 14a. Indeed, for the wavevector $\mathbf{q} = (16, 0)2\pi/L$, there are $8 + 1$ of these sequences below the spinwave peak, including the ones that contribute only at $\omega = 0$. The higher sequences are more spread out, and merge with the other ones, making a complicated fine structure in $S(\mathbf{q}, \omega)$. Similar features are seen in the MC-SD data, Fig. 14b, although it is clear that the individual peaks of each sequence are smeared out, resulting in one wider feature from the entire sequence.

Another example of these finite size features, for an odd integer wavevector, $\mathbf{q} = (9, 0)2\pi/L$ is shown in Fig. 18, again for $L = 128$ and $T = 0.3J$. For this smaller integer wavevector there are now only 5 sequences of fine-structure difference process peaks. It is significant that there is no such peak at zero frequency. This is clearly caused by the absence of any allowed spinwave difference process exactly at $\Omega_- = 0$, although there are many such processes with very weak weights *close* to $\Omega_- = 0$. In general, for any odd integer wavevector, $S(\mathbf{q}, \omega)$ will have a relative minimum at $\omega = 0$, because of the absence of allowed difference processes there.

In Fig. 18 we also show some of the weights of the sum-processes, $\Omega_+ = \omega_{\mathbf{k}} + \omega_{\mathbf{q}-\mathbf{k}}$, indicated by plus signs. For either sum or difference processes, numbers in parenthesis refer to the values of \mathbf{k} in units of $2\pi/L$. The sum frequencies must fall above the spinwave frequency $\omega_{\mathbf{q}}$. Comparing Figures 18 and 15, we see that the finite size features above $\omega_{\mathbf{q}}$ in $S(\mathbf{q}, \omega)$ can each be identified with a particular spinwave sum process. The identification, however, is somewhat more complex than that for the difference processes, because the different sequences of processes overlap in frequency. The match between the sum peak frequencies in the memory data and the MC-SD data is not as good as for the differences processes below $\omega_{\mathbf{q}}$. We can note that at these higher frequencies, any relative errors appear larger on an absolute scale, and, the spinwave sum/difference frequencies do not include any exchange softening effects.

Finally we show another example, for $\mathbf{q} = (5, 0)2\pi/L$ at $T = 0.1J$, $L = 128$ in Fig. 19, where both the difference and sum processes are shown. In this case there are only 3 dominant sequences of difference processes leading to finite size features.

D. Higher Temperature

Although the memory function formalism applied above, strictly speaking, applies to low temperatures, it is interesting to consider what kind of predictions it makes if applied at higher temperatures. It is clear from the above comparisons between MC-SD data and the memory function data that at low temperatures, where the

spinwave approximation should be valid, the damping of the modes has been underestimated. This is seen especially in the $T = 0.1J$ memory data where all the finite size features, as well as the spinwave peak, are too narrow. Thus it is interesting to see whether the spinwave width and shape are better described by this theory at higher temperature, because the theoretical damping rates grow as T^2 . The other reason to look at higher temperature is to consider how the background intensity in $S(\mathbf{q}, \omega)$ for frequencies $\omega < \omega_{\mathbf{q}}$, depends on the temperature. For one thing, the increase in temperature should spread all of the finite-size effect peaks and smooth the spinwave background, but can be expected to raise its intensity as well. For comparison, as T crosses the vortex unbinding temperature T_{BKT} , previous MC-SD simulations^{25,27,28} show that this background grows with T , until it dominates over the spinwave peak. The effect has been described by a theory employing a gas of freely moving vortices,³⁰ although simulations have given some indication that vortex lifetimes³¹ are rather too short to take this theory literally, and, vortices tend to be pinned by the lattice and also have complex motions not resembling free translation. Thus it is interesting to compare the memory approach to the MC-SD data at higher temperatures, where the latter will include effects due to all possible types of excitations, beyond linear spinwaves.

For $\lambda = 0$, the vortex unbinding temperature has been estimated to be $T_{\text{BKT}} \approx 0.7J$. In Fig. 20, we show some comparisons of the continuum ($L \geq 1024$) memory and MC-SD ($L = 128$) data for $S(\mathbf{q}, \omega)$, at temperatures $0.5J \geq T \geq 0.9J$ for two particular values of \mathbf{q} . As already seen, the spinwave peak locations in the MC-SD data here also fall lower than the memory function theory prediction. Also, there is a significant growth of the low-frequency background ($\omega < \omega_{\mathbf{q}}$) in the MC-SD data and in the memory function calculations. For $T = 0.9J$ the low-frequency background already dominates over the spinwave peak, if the latter can be seen at all. The effect is stronger in the MC-SD data: there is a clear excess of intensity around zero-frequency in $S(\mathbf{q}, \omega)$ in the MD-SD data compared to the memory function data. This effect is absent at $T \leq 0.5J$, however, where the MC-SD and memory data coincide for low frequencies; in this low temperature region the spinwave approximations used in the memory approach are valid. For temperatures near and above T_{BKT} , this extra central peak intensity, not described within the spinwave picture of the memory function approach, may possibly be attributed to nonlinear excitations, including specifically, vortices. This is consistent with the phenomenological vortex gas description of Mertens et al.³⁰ the excess central peak component is stronger for lower wavevectors, because the vortex pairs being generated above T_{BKT} disorder the spins on long length scales.

VII. DISCUSSION AND CONCLUSIONS

The presence of spinwave damping included into the memory function approach has been suggested here as a way in which finite amplitude spinwave peaks result in the 2D XY model, canceling the divergences in previous theories. A rough calculation of the damping strength has been made using the Feynmann diagram technique applied to the quartic corrections of the harmonic Hamiltonian. The diagrams used involve only two scattering events; clearly this gives an underestimate of the damping, and it is likely that including the third order diagrams could make a substantial modification to the results. Generally the damping $\Gamma_{\mathbf{k}}$ obtained increases away from the center of the Brilluoin zone, being close to zero near the center and being greatest along the (11) direction. In this classical calculation, the damping varies as the square of the temperature; this results in extremely weak damping strength ($\Gamma_{\mathbf{k}} \ll \omega_{\mathbf{k}}$) for temperatures below $0.3J$. As the temperature approaches and passes T_{BKT} , the damping becomes comparable to the spinwave frequency.

The comparison of the memory function data and MC-SD data for $S(\mathbf{q}, \omega)$ is good in several aspects: the theory gives finite spinwave peaks, they are positioned correctly for low temperatures, and the multiple finite-size-effect peaks are reproduced as in the MC-SD data. The most significant problem in the memory function approach is the extremely narrow peak widths—clearly caused by an underestimate of the true damping strength, especially at lower temperatures and wavevectors. For very low temperatures in the present theory, the longest wavelength spinwaves will not scatter even once before crossing the entire system. Of course, this is a quantum picture, applied to the classical system, so perhaps a better approach in this low-T limit would be to consider some kind of adiabatic scattering in the nonuniform potential due to the spinwave population. This would essentially be the equivalent of the quantum calculation at very high order diagrams rather than at the lowest order.

When the memory calculation is carried out for large systems, that is, in the continuum limit, the finite-size peaks merge into a smooth background. Indeed, in this limit, the spinwave peak itself has contributions on the high frequency side from spinwave sum processes, and on the low frequency side from spinwave difference processes. The combination of all of these contributions, essentially an infinite number of sum and difference processes, leads to an overall smooth and nondivergent spinwave peak. Even in the limit of *zero damping*, the spinwave peak are nondivergent, according to continuum calculations [using Eqs. 67] by Pereira et al.¹⁹ However, when damping is included, the heights of the spinwave peaks are smaller, and we expect the results to be more realistic.

In the memory function theory, the spinwave peak height was seen to be proportional to $[\text{Im}\Sigma(\omega_{\text{peak}})]^{-1}$. The function $\Sigma(\mathbf{q}, \omega)$, to a leading approximation, is pro-

portional to the temperature T . From Eq. (50), in regions away from the spinwave peak $S(\mathbf{q}, \omega)$ should be proportional to $\Sigma(\mathbf{q}, \omega)$. Thus we see that the memory function theory demonstrates how the background grows with temperature while the spinwave peak relatively tends to fall. For high enough temperature, the distribution of spinwave difference processes near zero frequency dominates the spectrum of $S(\mathbf{q}, \omega)$, leading to a central peak stronger than the spinwave peak. Clearly this means applying the theory well above the limiting temperature where we expect spinwave approximations to be valid. However, this gives results very similar to those in the MC-SD simulations, although the latter can be expected to include nonlinear effects such as vortices. In fact, we have seen a strong indication for nonlinear effects (beyond spinwave difference processes) above T_{BKT} as extra intensity in $S(\mathbf{q}, \omega)$ near zero frequency in the MC-SD data.

In conclusion, application of the memory function formalism, including a leading approximation to the mode damping, has been shown to accomplish three things for the XY model: i) produce nondivergent spinwave peaks; ii) explain the finite size features in $S(\mathbf{q}, \omega)$ both above and below $\omega_{\mathbf{q}}$; iii) explain the background in $S(\mathbf{q}, \omega)$ below $\omega_{\mathbf{q}}$ for the infinite system. Note that strictly speaking, damping is necessary only for item ii), because $S(\mathbf{q}, \omega)$ cannot be calculated in the memory function formalism for a finite system without damping. The continuum memory function approach gives finite size spinwave peaks and a low-frequency background even in the absence of damping. The theory also suggests that a sizable contribution to the growth of the central peak for T above T_{BKT} may be due to spinwave difference processes. The excess central peak intensity in the MC-SD data, when compared to the memory function data, must be due to nonlinear excitations, and gives evidence for dynamical effects due to vortices.

Acknowledgments.—GMW thanks Universidade Federal de Minas Gerais for their hospitality and support on this project. The authors thank the support by NSF-INT-9502781, NSF CDA-9724289, FAPEMIG, and CNPq.

- ⁵ J. M. Kosterlitz and D. J. Thouless, *J. Phys. C* **6**, 1181 (1973)
⁶ R. D. Mattuck, *A Guide to Feynmann Diagrams in the Many-Body Problem*, McGraw-Hill International Book Company (1976).
⁷ A. L. Fetter and J. D. Walecka, *Quantum Theory of Many-Particle Systems*, McGraw-Hill, New York (1971).
⁸ A. A. Abrikosov, L. P. Gorkov and I. E. Dzyaloshinski, *Quantum Field Theoretical Methods in Statistical Physics*, Pergamon Press, Oxford (1965).
⁹ G. Gilat and J. Raubenheimer, *Phys. Rev.* **144**, 390 (1966).
¹⁰ G. Gilat and Z. Kam, *Phys. Rev. Lett.* **22**, 715 (1969).
¹¹ G. Gilat, *J. Comp. Phys.* **10**, 432 (1972).
¹² In two-dimensions, Eq. (44) becomes

$$D_{\text{cell}}(\omega) = \frac{f(x_c)}{|\nabla g(x_c)|} \frac{1}{2|l_1 l_2|} \sum_{i=1}^4 (-1)^{m_i} |w + w_i|, \quad (71)$$

and in three dimensions,

$$D_{\text{cell}}(\omega) = \frac{f(x_c)}{|\nabla g(x_c)|} \frac{1}{4|l_1 l_2 l_3|} \sum_{i=1}^8 (-1)^{m_i} |w + w_i| (w + w_i). \quad (72)$$

For arbitrary dimension d , the generalization is

$$D_{\text{cell}}(\omega) = \frac{f(x_c)}{|\nabla g(x_c)|} \frac{1}{2(d-1)!|l_1 l_2 \dots|} \sum_{i=1}^{2^d} (-1)^{m_i} \frac{(w + w_i)^d}{|w + w_i|} \quad (73)$$

- ¹³ G. Reiter and A Sjölander, *Phys. Rev. Lett.* **39**, 1047 (1977); *J. Phys. C: Solid State Phys.* **13** 3027 (1980).
¹⁴ H. Mori, *Prog. Theor. Phys.* **33**, 423 (1965).
¹⁵ B. De Raedt, H. De Raedt and J. Fizez, *Phys. Rev. B* **23**, 4597 (1981).
¹⁶ M. E. Gouvêa and A. S. T. Pires, *J. Phys. C: Solid State Phys.* **20**, 2431 (1987).
¹⁷ S. Menezes, A. S. T. Pires and M. E. Gouvêa, *Phys. Rev. B* **47**, 12280 (1993).
¹⁸ A. F. A. Pereira, M. S. thesis, Universidade Federal de Minas Gerais, Brazil (1999).
¹⁹ A. F. A. Pereira, M. E. Gouvêa and G. M. Wysin, unpublished.
²⁰ The usual conversion from discrete to continuum Fourier weights is to divide by the volume $(2\pi/L)^2$ per allowed point in \mathbf{q} -space:

$$F(\mathbf{q}) = \left(\frac{L}{2\pi}\right)^2 F_{\mathbf{q}} \quad (74)$$

- ²¹ The $1/\sqrt{N}$ normalization of the Fourier transform definition (9) simplifies many formulas in this paper, including the N -independent discrete correlation (52). Distributing this weight over the \mathbf{q} -space volume $d^2 q = (2\pi/L)^2$, leads to an N -dependent continuum correlation $S^{\perp\perp}(\mathbf{q}) = N(2\pi)^{-2} \langle S_{\mathbf{q}}^{\perp} S_{-\mathbf{q}}^{\perp} \rangle$. To avoid this N -dependence in the continuum quantity, it is only necessary to use the alternative Fourier transform definitions,

$$\phi_{\mathbf{n}} = \sum_{\mathbf{q}} \phi_{\mathbf{q}} e^{i\mathbf{q}\cdot\mathbf{n}}, \text{ etc.} \quad (75)$$

* Permanent Address: Department of Physics, Kansas State University, Manhattan, KS 66506-2601. [email: wysin@phys.ksu.edu].

¹ J. Villain, *J. Phys. (Paris)* **35**, 27 (1974).

² F. Moussa and J. Villain, *J. Phys. C* **9**, 4433 (1976).

³ D. R. Nelson and D. S. Fisher, *Phys. Rev. B* **16**, 4945 (1977).

⁴ V. L. Berezinskii, *Sov. Phys. JETP* **32**, 493 (1970); **34**, 610 (1972).

This would complicate many intermediate formulas, but in the end the continuum $S(\mathbf{q}, \omega)$ will be independent of N and also have a prefactor of $(2\pi)^{-2}$.

- ²² G. M. Wysin, unpublished.
²³ M. E. Gouvêa, unpublished.
²⁴ M. E. Gouvêa and G. M. Wysin, Phys. Rev. B **56**, 14192 (1997).
²⁵ C. Kawabata, M. Takeuchi and A.R. Bishop, J. Magn. Mater. **54-57**, 871 (1986); J. Stat. Phys. **43**, 869 (1986); G.M. Wysin and A.R. Bishop, Phys. Rev. B **42**, 810 (1990);
²⁶ U. Wolff, Nucl. Phys. **B300**, 501 (1988); Phys. Rev. Lett. **62**, 361 (1989).
²⁷ Evertz and D.P. Landau, Phys. Rev. B **54**, 12302 (1996).
²⁸ D. P. Landau, J. Mag. Magn. Mater. **200**, 231 (1999); M. Krech and D. P. Landau, Phys. Rev. B **60**, 3375 (1999).
²⁹ M. E. Gouvêa, G. M. Wysin, S. A. Leonel, A. S. T. Pires, T. Kampeter and F. G. Mertens, Phys. Rev. B **59**, 6229 (1999).
³⁰ F.G. Mertens, A.R. Bishop, G.M. Wysin and C. Kawabata, Phys. Rev. B **39**, 591 (1989).
³¹ D.A. Dimitrov and G.M. Wysin, Phys. Rev. B **53**, 8539 (1996); J. Phys. C **10**, 7453-65 (1998).

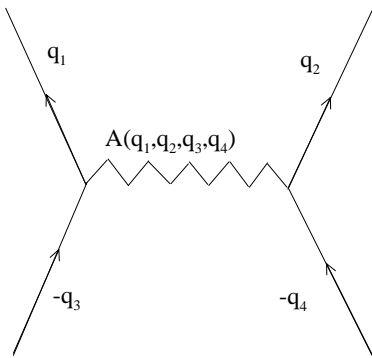


FIG. 1. Notation for the representation of the interaction terms in H_1 , Eq. (17), in the Feynmann diagrams.

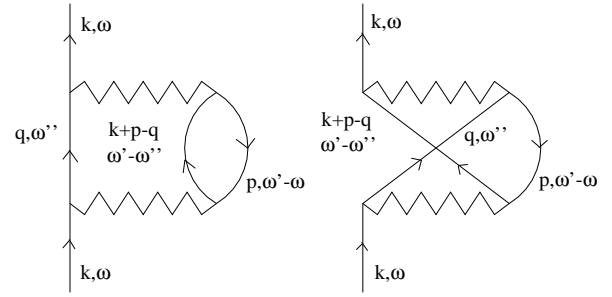


FIG. 2. The two leading diagrams that contribute to $G_2(\mathbf{k}, \omega)$, as in Eqs. (24) and (25).

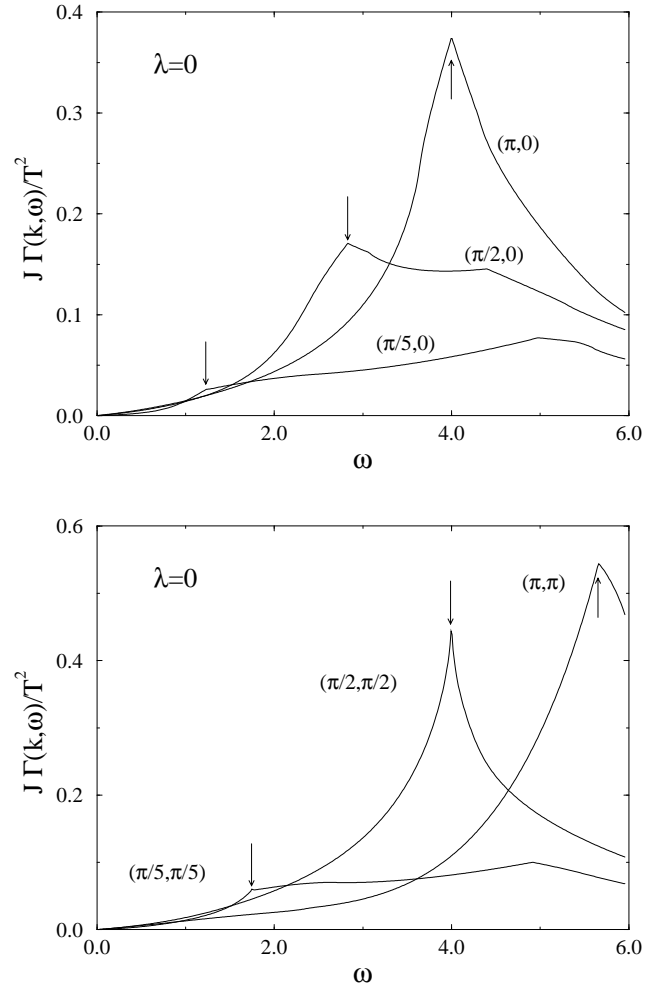


FIG. 3. Typical numerical results for the damping function $\Gamma(\mathbf{k}, \omega)$ at $\lambda = 0$, at various wavevectors as indicated. The arrows mark the positions of the spinwave frequency $\omega_{\mathbf{k}}$, for each associated wavevector.

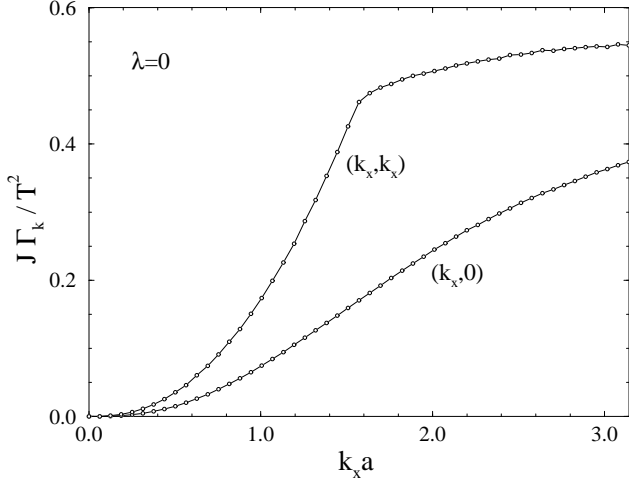


FIG. 4. The damping rate $\Gamma_{\mathbf{k}}$ for $\lambda = 0$ in the (10) and (11) directions.

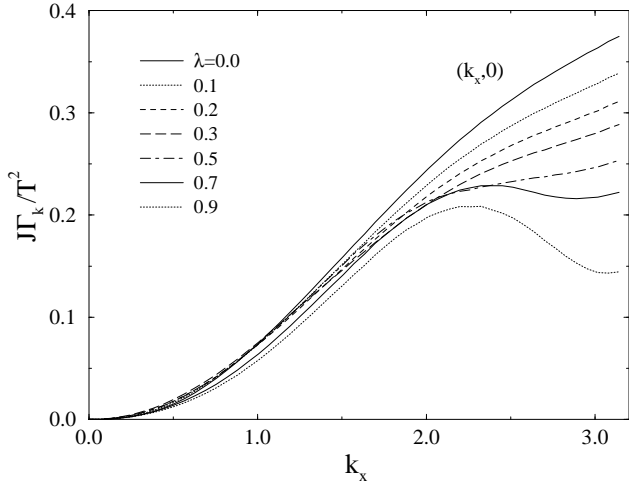


FIG. 5. The damping rate $\Gamma_{\mathbf{k}}$ for $0 \leq \lambda \leq 0.9$ in the (10) direction.

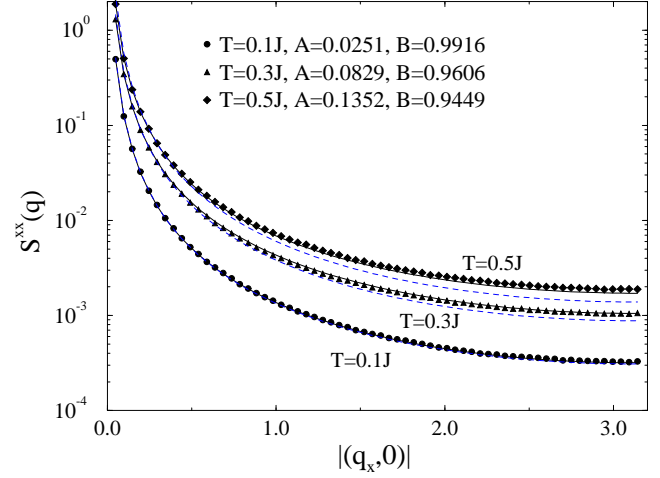


FIG. 6. Static correlation function for $\lambda = 0$, calculated from MC simulations for $L = 128$ (symbols), with fits to formula (69) (solid curves), compared to the low-temperature expression (52) (dashed curves).

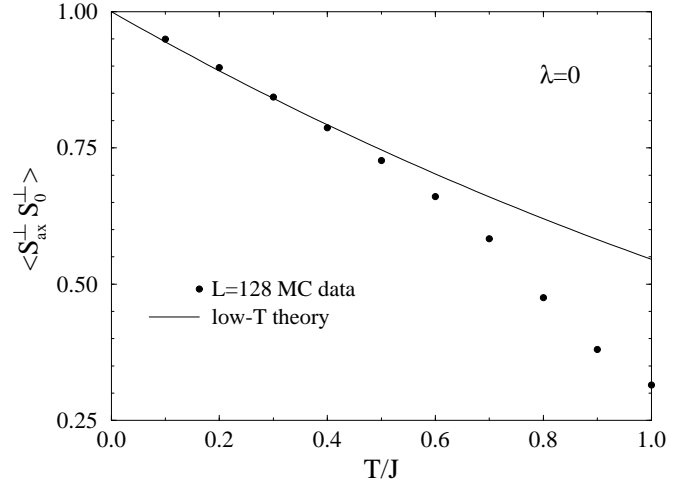


FIG. 7. Static nearest neighbor correlation function for $\lambda = 0$, calculated from MC simulations for $L = 128$ using Eq. (54) (symbols), compared to the low-temperature expression (55) (solid curve).

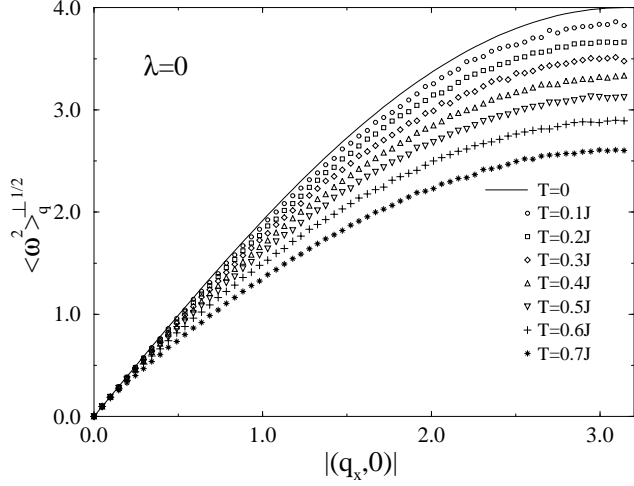


FIG. 8. The second moment vs. \mathbf{q} for $\lambda = 0$, at the temperatures indicated, using the data from $L = 128$ MC simulations, compared with the zero-temperature dispersion relation (solid curve).

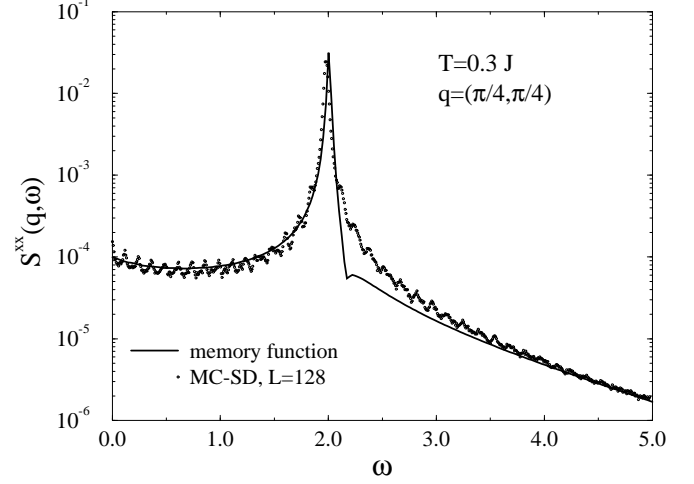


FIG. 10. The dynamical structure function obtained from the memory function of Fig. 9 (solid curve), calculated using $L = 2048$ for $T = 0.3J$, $\mathbf{q} = (\pi/4, \pi/4)$. compared with MC-SD data (symbols) for the $L = 128$ system. The frequency resolution of the SD data here and in Figs. 11, 12, 13 is $\Delta\omega = 0.0046484JS$.

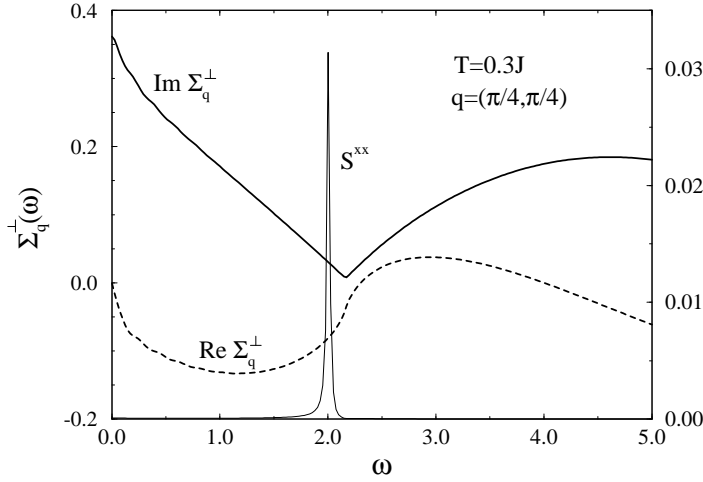


FIG. 9. Real and imaginary parts of the memory function $\Sigma_{\mathbf{q}}^{\perp}(\omega)$, calculated using $L = 2048$ for $T = 0.3J$, $\mathbf{q} = (\pi/4, \pi/4)$, and the resulting dynamical structure function $S^{xx}(\mathbf{q}, \omega)$.

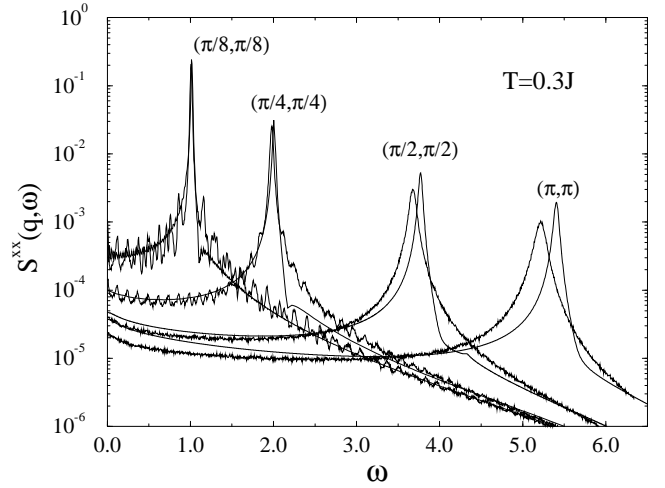
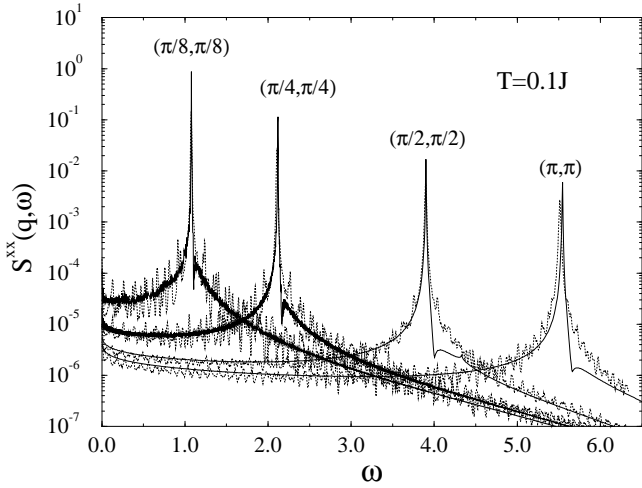
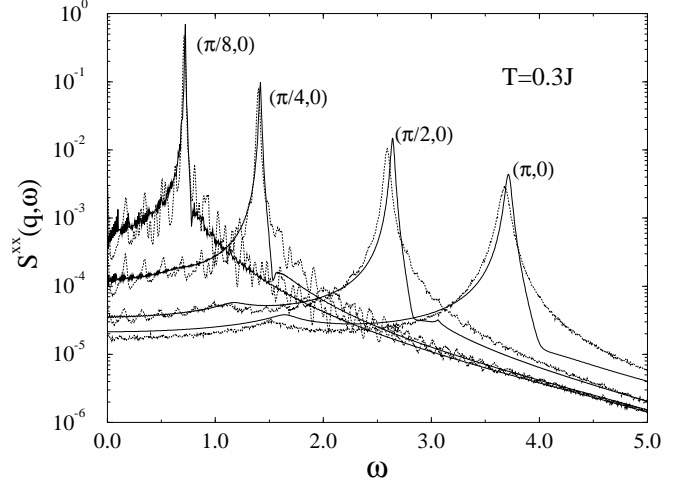
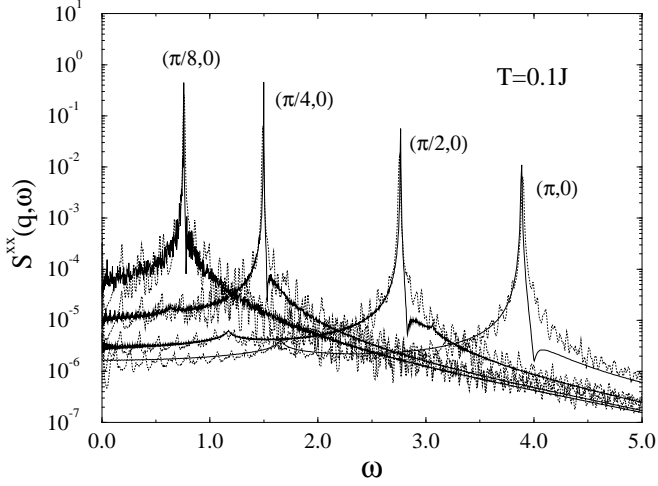


FIG. 11. The $T = 0.1J$ dynamical structure function obtained from the memory function calculations (solid, using $L = 2048-4096$) and MC-SD simulations (dotted) for the $L = 128$ system, at wavevectors indicated in parenthesis. The memory data and the MC-SD data are both smeared by finite-size effects, even for these large L .

FIG. 12. The $T = 0.3J$ dynamical structure function obtained from the memory function calculations (solid curves, using $L = 1024-2048$) compared with MC-SD data (dotted curves) for the $L = 128$ system. The peaks in the MC-SD data fall at slightly lower frequencies than the memory predictions.

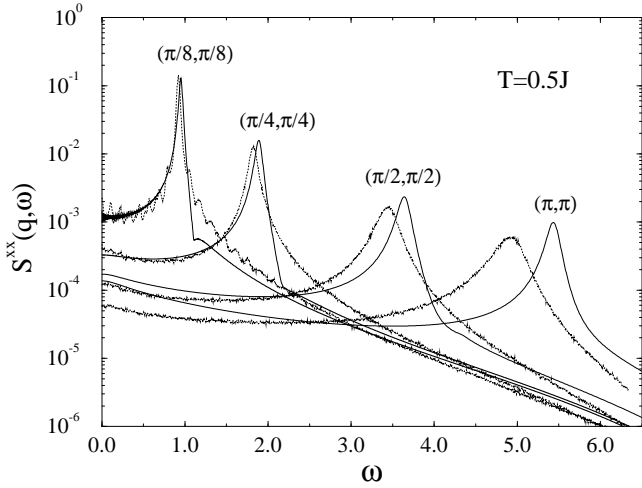
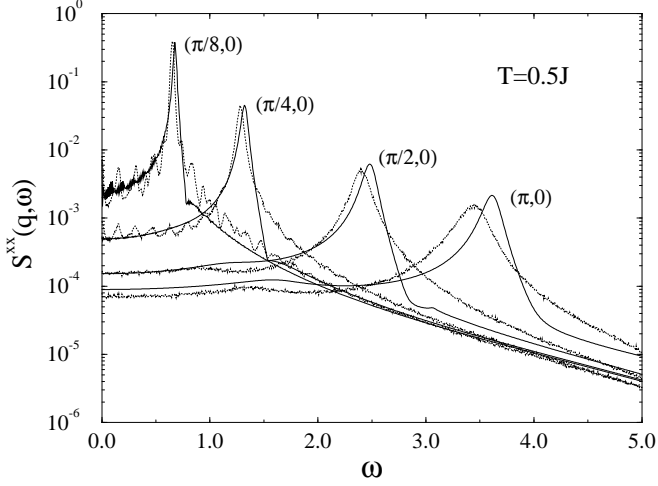


FIG. 13. The $T = 0.5J$ dynamical structure function obtained from the memory function calculations (solid curves, using $L = 1024-2048$) compared with MC-SD data (dotted curves) for the $L = 128$ system.

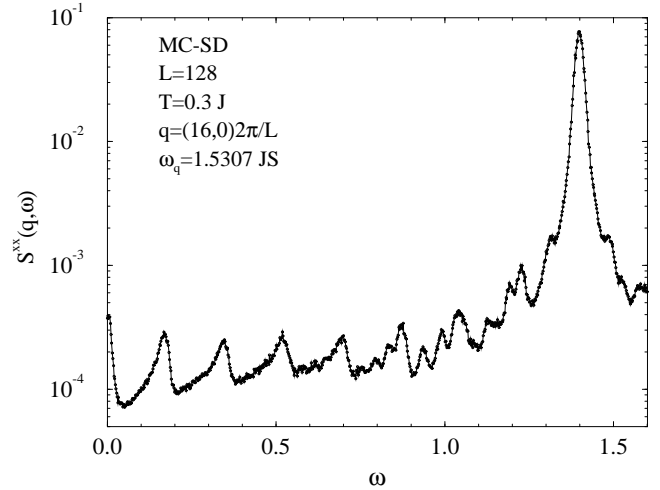
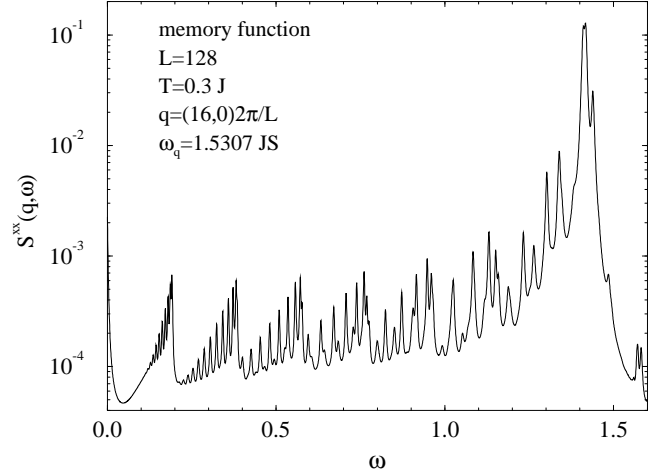


FIG. 14. Sequences of finite-size features in the dynamic structure function for an even integer wavevector, $\mathbf{q} = (16, 0)2\pi/L$, at $T = 0.3J$, from a) the memory function approach, and b) the Monte Carlo Spin-Dynamics. The frequency resolution of the SD data here and in Figs. 15, 16 is $\Delta\omega = 0.0018262JS$.

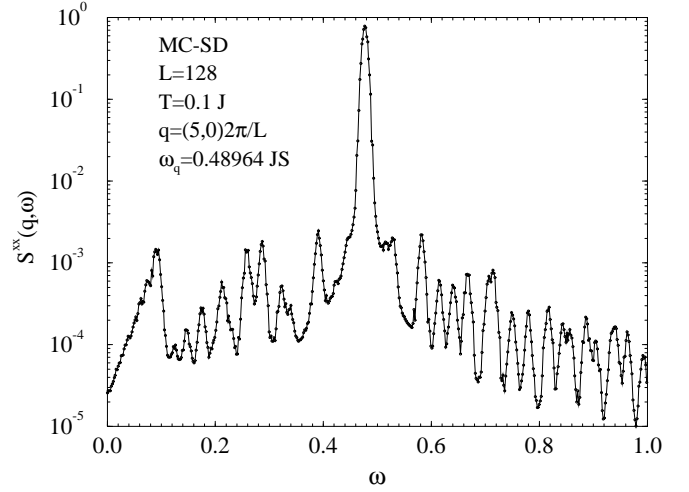
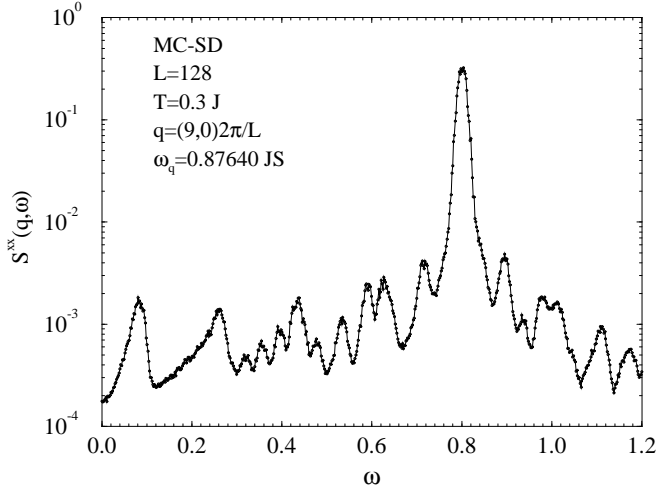
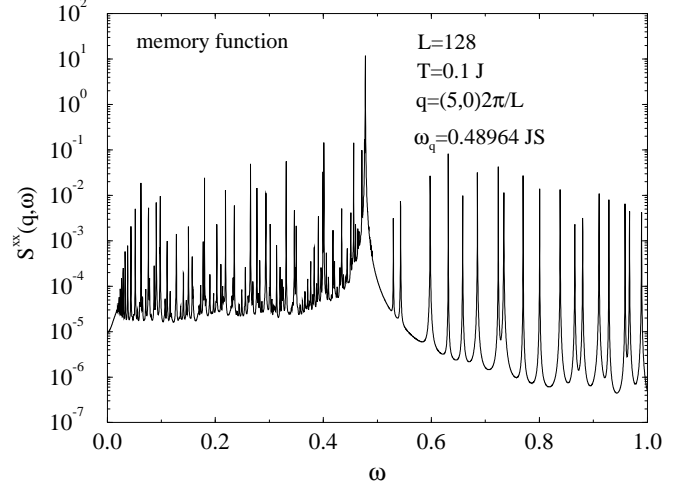
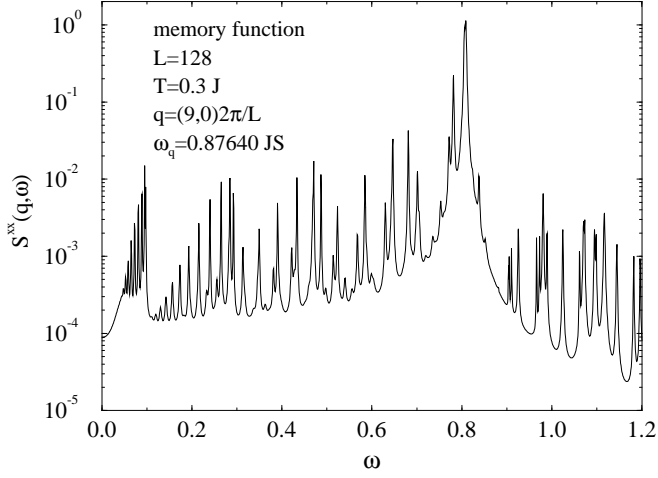


FIG. 15. Dynamic structure function for an odd integer wavevector, $\mathbf{q} = (9, 0)2\pi/L$, at $T = 0.3J$, from a) the memory function approach, and b) the Monte Carlo Spin-Dynamics.

FIG. 16. Dynamic structure function for an odd integer wavevector, $\mathbf{q} = (5, 0)2\pi/L$, at $T = 0.1J$, from a) the memory function approach, and b) the Monte Carlo Spin-Dynamics.

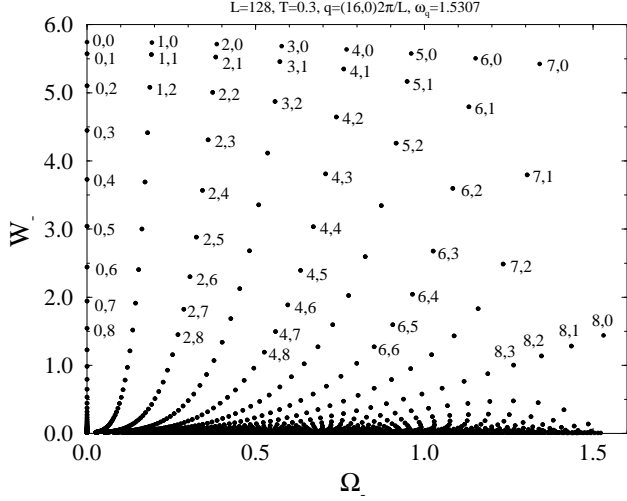


FIG. 17. Plot of difference process weights versus spin-wave difference frequency $\Omega_- = \omega_{\mathbf{k}} - \omega_{\mathbf{q}-\mathbf{k}}$ for the $L = 128$ system, for an even integer wavevector $\mathbf{q} = (16,0)(2\pi/L)$, at $T = 0.3J$, showing sequences of difference processes with high weights, responsible for the sequences of finite size features in Fig. 14. Numbers in parenthesis are wavevector values \mathbf{k} in units of $2\pi/L$.

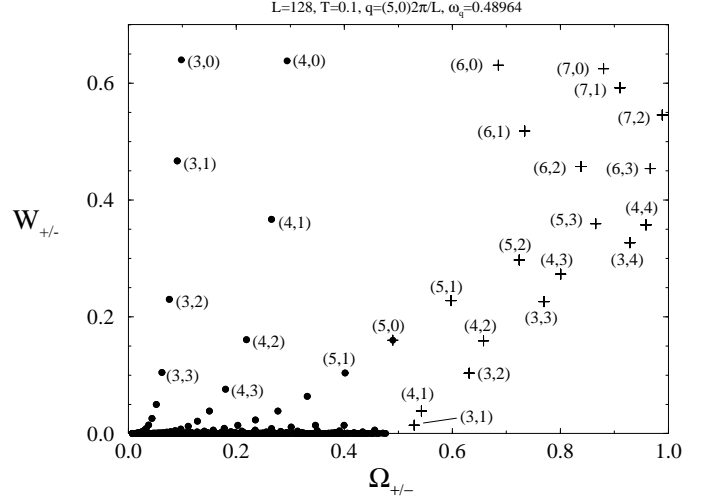


FIG. 19. Sum (+ signs) and difference (solid circles) process weights versus frequencies $\Omega_{\pm} = \omega_{\mathbf{k}} \pm \omega_{\mathbf{q}-\mathbf{k}}$ for the $L = 128$ system, for an odd integer wavevector $\mathbf{q} = (5,0)(2\pi/L)$, at $T = 0.1J$. Compare the locations of the features in Fig. 16. Numbers in parenthesis are wavevector values \mathbf{k} in units of $2\pi/L$.

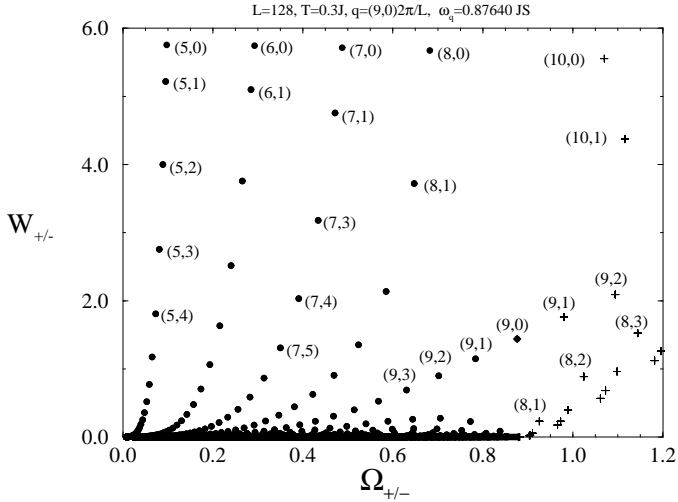


FIG. 18. Sum (+ sigms) and difference (solid circles) process weights versus frequencies $\Omega_{\pm} = \omega_{\mathbf{k}} \pm \omega_{\mathbf{q}-\mathbf{k}}$ for the $L = 128$ system, for an odd integer wavevector $\mathbf{q} = (9,0)(2\pi/L)$, at $T = 0.3J$. Compare the locations of the features in Fig. 15. Numbers in parenthesis are wavevector values \mathbf{k} in units of $2\pi/L$.

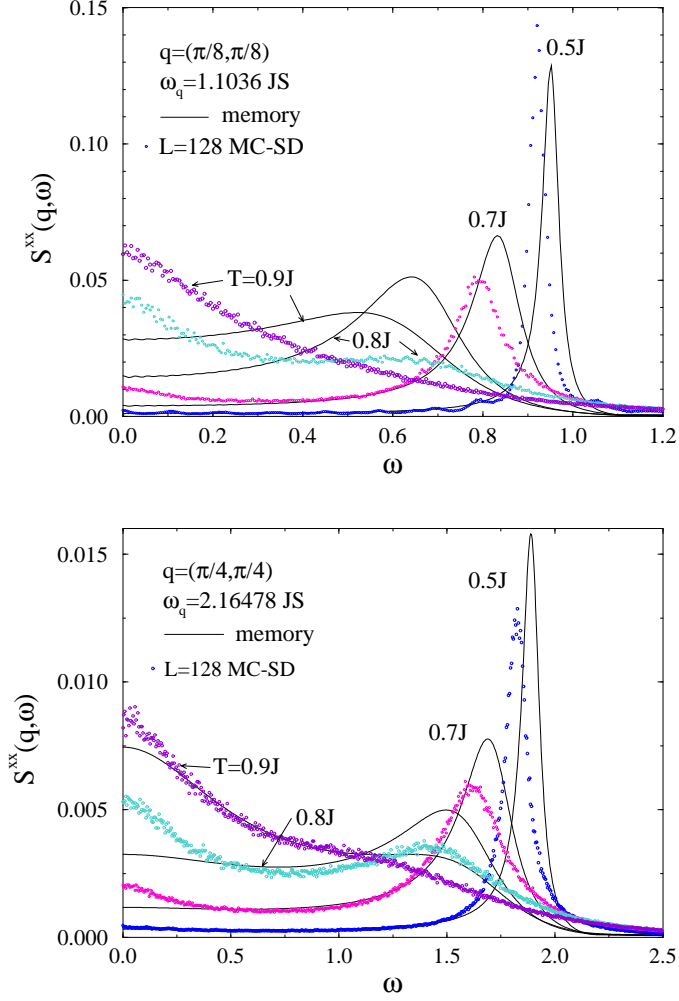


FIG. 20. Dynamic structure function at wavevectors $\mathbf{q} = (\pi/8, \pi/8)$ and $\mathbf{q} = (\pi/4, \pi/4)$, from the memory calculations (solid curves) compared to Monte Carlo Spin-Dynamics (data points) on $L = 128$ systems, for a range of higher temperatures.